



The Eocene–Oligocene Transition in the Paratethys: boreal water ingressions and its paleoceanographic implications

Mustafa Yücel Kaya^{1,a}, Henk Brinkhuis^{2,3}, Chiara Fioroni⁴, Serdar Görkem Atasoy¹, Alexis Licht⁵, Dirk Nürnberg⁶, and Taylan Vural¹

¹Department of Geological Engineering, Middle East Technical University, Ankara, 06800, Türkiye

²Oceans Systems Research (OCS), NIOZ Royal Netherlands Institute of Sea Research, Texel, 1790 AB, the Netherlands

³Department of Earth Sciences, Laboratory of Palaeobotany and Palynology, Faculty of Geosciences, Utrecht University, 3584 CB Utrecht, the Netherlands

⁴Dipartimento di Scienze Chimiche e Geologiche, Università degli Studi di Modena e Reggio Emilia, Modena, 41121, Italy

⁵Aix-Marseille Université, CNRS, IRD, INRAE, Collège de France, CEREGE, Technopôle de l'Arbois-Méditerranée, BP80, 13545 Aix-en-Provence, France

⁶GEOMAR Helmholtz Centre for Ocean Research Kiel, 24148 Kiel, Germany

^apresent address: Geological Institute, RWTH Aachen University, Aachen, Germany

Correspondence: Mustafa Yücel Kaya (mustafayk@gmail.com)

Received: 3 February 2025 – Discussion started: 18 February 2025

Revised: 5 May 2025 – Accepted: 26 May 2025 – Published: 1 August 2025

Abstract. The Eocene–Oligocene Transition (EOT) represents a pivotal period in Earth's climatic history, marked by the onset of Antarctic glaciation and global cooling. While deep-sea records have extensively documented this transition, its impacts on marginal and epicontinental seas remain less understood. This study investigates the impacts of the EOT in the Karaburun composite section, located in the Eastern Paratethys. Using a multidisciplinary approach that integrates biostratigraphy, geochemistry, geochronology, and sequence stratigraphy, a robust chronostratigraphic framework for the latest Eocene to early Oligocene was established. The stable isotopic shifts observed in benthic and planktic foraminifera $\delta^{18}\text{O}$ and $\delta^{13}\text{C}$ records at Karaburun align with global patterns but also reveal regional effects, such as freshwater influx and basin restriction, specific to the semi-restricted Paratethys. The abrupt negative $\delta^{18}\text{O}$ shift across the Eocene–Oligocene Boundary (EOB) in the Paratethys reflects boreal water ingressions driven by the onset of anti-estuarine circulation between the Nordic Seas and the Atlantic and the closure of the Arctic–Atlantic gateway, which redirected cold, low-salinity boreal waters through interconnected basins towards the Paratethys. These findings highlight the interplay between global climate drivers and regional hydrological dynamics, providing critical in-

sights into the evolution of marginal marine environments during the EOT. Our results underscore the significance of the Paratethys as a unique archive for studying the onset of global icehouse climate conditions and regional responses.

1 Introduction

The Earth's geological history has witnessed several significant long-term climate transitions, along with short-term disruptions to the carbon cycle. The most recent of these transitions occurred over the last 50 million years during the Cenozoic and is characterized by a long-term cooling trend and a decline in atmospheric CO_2 levels, culminating in the onset of Antarctic glaciation during the Eocene–Oligocene Transition (EOT) (e.g., Zachos et al., 2001; Caves et al., 2016). The EOT marks the end of an extended period of predominantly greenhouse conditions and represents a phase of accelerated biotic change lasting approximately 500–800 kyr, bracketing the Eocene–Oligocene Boundary (EOB) (Coxall and Pearson, 2007; Hutchinson et al., 2021). This transition is also associated with a deepening of the ocean's calcite compensation depth (CCD) (Coxall et al., 2005), a northward migration of the Intertropical Convergence Zone (ITCZ) (Hyeong

et al., 2016), and increased seasonality in northern high latitudes (Eldrett et al., 2009).

The Antarctic glaciation events during the Oligocene are referred to as Oi events (Pälike et al., 2006; Pekar and Miller, 1996). At deep-ocean sites Oi glaciation events are characterized by positive excursions in the oxygen isotope records of benthic foraminifera (Miller et al., 1991; Pälike et al., 2006; Wade and Pälike, 2004). During the earliest Oligocene there are two significant cooling/glaciation events: (1) Oi-1 (Early Oligocene Glacial Maximum, EOGM of Hutchinson et al., 2021) and (2) Oi-1a, corresponding to early part of paleomagnetic Subchron C12r, took place during the early Rupelian (Pekar et al., 2002, and references therein). The EOGM, spanning 490 kyr from ~ 33.65 to 33.16 Ma, marks a sustained period of cold climate and glaciation during paleomagnetic Subchron C13n (Hutchinson et al., 2021). The Oi-1a glaciation event corresponds to the appearance of the cold-water dinocyst taxa *Svalbardella cooksoniae* and/or *Svalbardella* spp. in the North Sea Basin (Śliwińska, 2019, and references therein). Episodes of southward migration of *Svalbardella cooksoniae* have consequently been interpreted as evidence of cooling events (e.g., Van Simaey et al., 2005). *Svalbardella cooksoniae* has also been documented in a brief interval during the earliest Oligocene at numerous sites across the Northern Atlantic and Western Tethyan regions (Śliwińska and Heilmann-Clausen, 2011).

The most comprehensive insights into the EOT come from deep-sea marine records of benthic foraminiferal oxygen and carbon isotopes ($\delta^{18}\text{O}$ and $\delta^{13}\text{C}$), extensively analyzed using cores from the Deep Sea Drilling Project (DSDP), Ocean Drilling Program (ODP), and Integrated Ocean Discovery Program (IODP) (e.g., Zachos et al., 1996; Pekar and Miller, 1996; Salamy and Zachos, 1999; Coxall et al., 2005; Bordiga et al., 2015; Hutchinson et al., 2021, and references therein). In contrast, changes associated with the EOT in marginal and epicontinental seas have been the focus of relatively few studies (e.g., Pearson et al., 2008; Ozsvárt et al., 2016; van Der Boon et al., 2019; Dickson et al., 2021). Nevertheless, geochemical and sedimentary data from these shallow regions can offer valuable insights into the impacts of the EOT, including Antarctic glaciation and cooling, within restricted marine environments influenced by local factors such as freshwater influx, salinity variations, weathering, erosion, and terrestrial (sediment and carbon) fluxes.

This study addresses the gap in understanding the EOT conditions in epicontinental seas by revisiting and reanalyzing an Eocene–Oligocene Boundary (EOB) section in the Karaburun area of northern Türkiye (Fig. 1a). The Karaburun section with its exceptionally well-preserved and diverse assemblages of microfossils (e.g., Simmons et al., 2020; Sancay and Bati, 2020) provides an excellent opportunity to investigate the distribution of key latest Eocene–earliest Oligocene organic walled dinoflagellate cyst (dinocyst) and calcareous nannofossil index species. Furthermore, it sheds light on how climatic changes influenced stratigraphic se-

quences in the Eastern Paratethys Sea – the largest Cenozoic epicontinental sea, with no modern analogue. To investigate these processes, the EOB section at Karaburun is analyzed using marine palynology emphasizing dinocysts and calcareous nannofossil biostratigraphy, as well as high-resolution stable oxygen and carbon isotope analyses of benthic (*Cibicidoides* spp.) and planktic (*Turborotalia ampliapertura*) foraminifera. U–Pb dating of a tuff layer within the section further constrained the age model, complementing the biostratigraphic and chemostratigraphic data, as well as allowing sequence stratigraphic interpretations. The findings are compared with the EOT records from other Paratethys sites and global oceans to discern the regional and global climatic and oceanographic effects.

2 Geological setting

The interplay of paleoclimatic and tectonic processes fragmented the largely enclosed Paratethys water body into numerous subbasins, separated by narrow, shallow gateways and land bridges (Palcu and Krijgsman, 2023). Extending from southern Germany to China (Fig. 1b), the Paratethys encompassed three distinct regions. The Western and Central Paratethys are characterized by active tectonics and comprised smaller, short-lived basins. The Western Paratethys included the western Alpine foreland basin, while the Central Paratethys included subbasins spanning from Austria to Romania (e.g., Popov et al., 2004). In contrast, the Eastern Paratethys, centered around the Black Sea and Caspian Sea basins, evolved within a tectonically stable region (Popov et al., 2004).

The Karaburun area is situated along the southern margin of the Western Black Sea Basin, a back-arc basin formed during the late Cretaceous as a subbasin of the Paratethys Sea (Okay and Nikishin, 2015) (Fig. 1c). Since its formation, the Western Black Sea Basin has experienced continuous subsidence, resulting in a sedimentary thickness exceeding 14 km (Okay et al., 2019). To the south of the Karaburun area lies the Thrace Basin (Fig. 1a), which is younger and characterized by Eocene–Oligocene clastic fill deposits, reaching a maximum thickness of approximately 9 km in its central region (Turgut, 1991). During the Eocene and Oligocene, the Strandja Massif – a polydeformed, deeply eroded orogenic belt composed of metamorphic and magmatic rocks – formed a paleo-high that separated the Western Black Sea Basin from the Thrace Basin to the south (Cattò et al., 2018) (Fig. 1a). The only marine connection between these basins was through the Çatalca Gap (Fig. 1a), located west of İstanbul, where sedimentation abruptly ceased during the early Oligocene due to an uplift event (Okay et al., 2019). This region represents the sole contact point between the Eocene–Oligocene sequences of the Black Sea and Thrace basins (Okay et al., 2019).

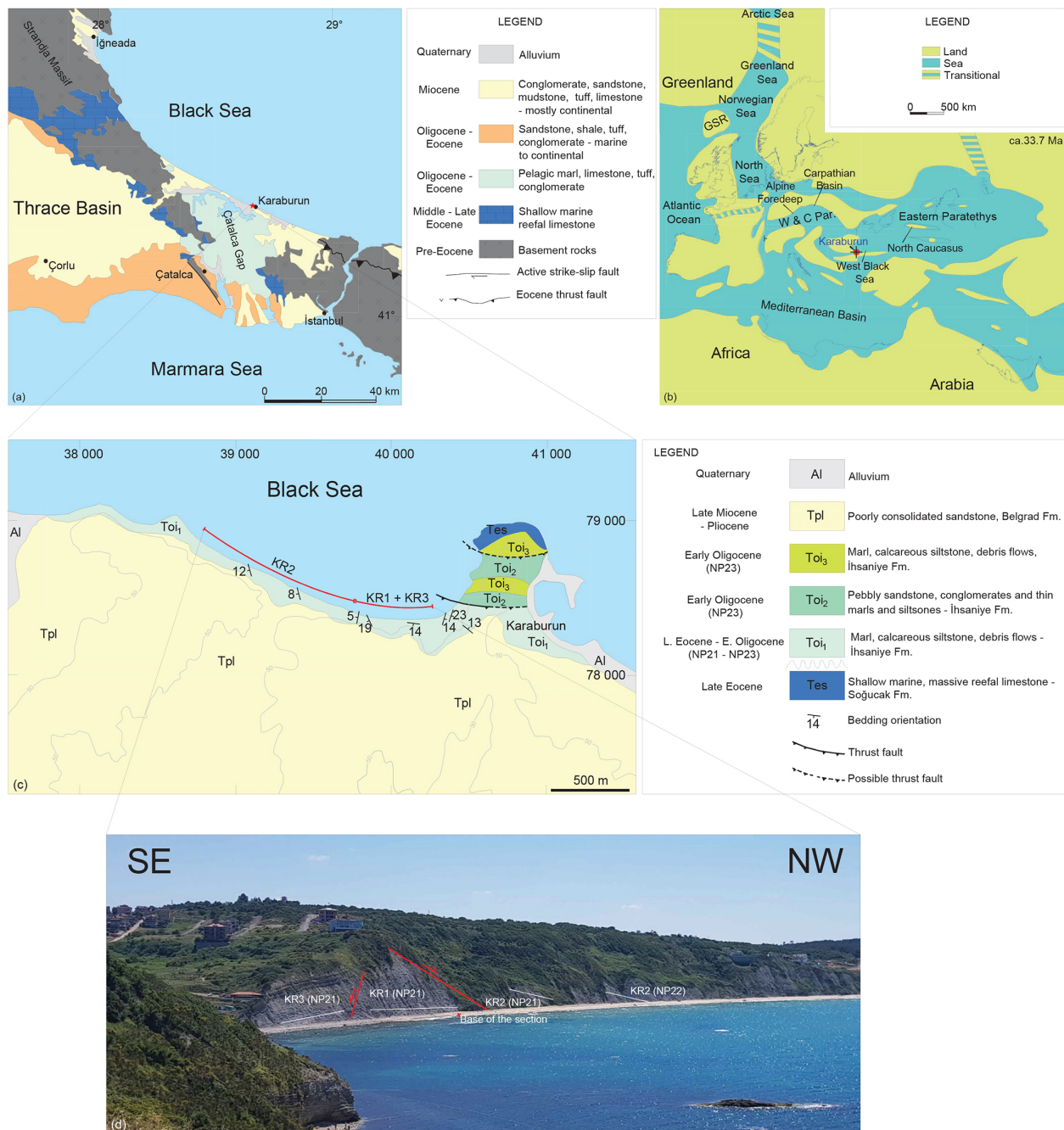


Figure 1. (a) Geological map of the Thrace region (Türkiye) showing the location of the Karaburun area in relation to Thrace Basin, Strandja Massif, and Çatalca Gap (modified from Okay et al., 2020). (b) Paleogeography of the Paratethys during the early Oligocene (Rupelian, 33.7 Ma) (modified from Sachsenhofer et al., 2018). GSR: Greenland–Scotland Ridge. W & C Par.: Western and Central Paratethys. Red dot marks the Karaburun area. (c) Geological map of the Karaburun area showing the locations of the subsections KR1, KR2, and KR3 (revised from Okay et al., 2019). (d) View of the studied subsections facing south from Cape Karaburun.

3 Regional stratigraphy

The Soğucak Formation, characterized by shallow marine, massive reefal limestone, underlies the uppermost Eocene–lowermost Oligocene hemipelagic deposits in both the Thrace Basin and the Karaburun area (Fig. 1b). In the

Karaburun area, the Soğucak Formation has been dated to the Priabonian based on benthic foraminiferal biozonation (Yücel et al., 2020). Overlying this formation is a 120 m thick sedimentary succession from the latest Eocene to early Oligocene, predominantly composed of hemipelagic marls

and carbonates (Fig. 1c). This sequence also includes intermittent submarine fan deposits, debris flows, slumps, pebbly sandstones, and conglomerates near the top. A prominent tuff layer within this succession is linked to a significant Ruppelian volcanic event originating from the Rhodope Massif (Marchev et al., 2024). Although the hemipelagic succession in the Karaburun area has often been referred to as the Ceylan Formation – following the terminology used in the Thrace Basin (e.g., Natal'in and Say, 2015) – we adopt the designation “İhsaniye Formation”, as recommended by Okay et al. (2019) and Simmons et al. (2020). While prior studies assigned an early Oligocene age to the İhsaniye Formation in the Karaburun area (e.g., Less et al., 2011; Okay et al., 2019; Simmons et al., 2020), our findings refine its age to the latest Eocene–early Oligocene. This revision is based on the calcareous nannofossil and dinocyst biostratigraphy, stable oxygen and carbon isotope analyses, and U–Pb dating of the tuff layer.

4 Material and methods

4.1 Lithostratigraphy

Eocene and Oligocene deposits are well exposed in 50 m high cliffs along the Black Sea coast in the Karaburun area (Fig. 1d). These deposits have been the focus of recent studies (e.g., Okay et al., 2019; Sancay and Bati, 2020; Simmons et al., 2020; Tulan et al., 2020), which documented their paleoenvironment, biostratigraphy, and source rock potential. To build upon these studies, we revisited the area and measured three adjacent stratigraphic sections – designated as KR1, KR2, and KR3 (Fig. 1d). By integrating these sections, we constructed a composite Karaburun section comprising hemipelagic deposits of the İhsaniye Formation (Fig. 2).

The studied sediments predominantly consist of hemipelagic light-gray marls; dark-brownish clays; thin- to medium-bedded light-gray, whitish, and beige carbonates; calcareous siltstones; and sandstones, which occasionally display planar lamination. The sequence also includes submarine fan (turbiditic) conglomerates, as well as debris flow and slump deposits toward the top. The hemipelagic fine-grained deposits contain rich microfossil assemblages of planktic and benthic foraminifera, calcareous nannofossils, and dinocysts, indicating a latest Eocene–early Oligocene age (this study). The submarine fan deposits are characterized by thin to medium thick, erosive-based conglomeratic beds with mainly carbonate pebbles, organic matter, and microfossil fragments (e.g., foraminifera and shell debris) and intercalated with thin silty layers. They often grade vertically into sandstone layers. Although these submarine fan deposits exhibit variable lateral thicknesses, they provide solid key horizons for correlation of the subsections (e.g., correlation of the KR1 and KR3 subsections). Brownish organic-rich clay layers occasionally contain red-yellow nodules. Pyrite is commonly found in these

organic-rich layers. Additionally, pyritized coral fossils are rarely observed in these organic-rich clay deposits. A distinctive white tuff layer at approximately 71.5 m within the composite section was sampled for U–Pb zircon dating (see Sect. 4.5) (Fig. 2). Debris flow horizons, with a maximum thickness of 5 m, exhibit channel geometries and primarily consist of carbonate pebbles. These horizons increase in frequency toward the topmost 20 m of the succession. This study focuses on the lower and middle portions of the section including the EOT, ending around the tuff layer (Fig. 2), and does not include analysis of the uppermost part of the succession including the debris flow deposits.

4.2 Sequence stratigraphy

We analyzed various surfaces that indicate either a seaward or landward shift of successive facies belts, including erosive surfaces which could be equivalent to subaerial unconformities on land, transgressive surfaces, and maximum flooding surfaces. These surfaces demarcate the boundaries of different systems tracts – lowstand, transgressive, and highstand – which together form the depositional sequences (Catuneanu, 2006, and references therein).

In addition to the identification of the systems tracts based on the recognition of key surfaces, sedimentary facies and microfossil assemblages have been utilized to reconstruct past water depths and identify sea-level evolution, typically indicated by shifts towards offshore (or onshore) characteristics. The distribution and relative abundance of planktic and benthic foraminifera have further been employed to discern variations in relative sea level. Additionally, the relative abundance of lagoonal and inner neritic dinocysts, combined with the distribution patterns of associated brackish and terrestrial palynomorphs as well as the grain size of the deposited sediments, was examined to assess proximity to the coast.

4.3 Biostratigraphy

4.3.1 Calcareous nannofossils

The study on calcareous nannofossil assemblages was carried out on 84 samples, prepared at the Department of Earth Sciences of the University of Milan (Italy), following the smear-slide standard technique described by Bown and Young (1998). Calcareous nannofossils were analyzed using an Axioscope Zeiss light microscope (LM) at 1250X magnification. Preservation of the specimens was generally good, as indicated by the presence of holococcoliths, coccospheres, and small coccoliths. Quantitative analysis was performed by counting 300 specimens per sample, in a variable number of fields of view, depending on the nannofossil total abundance. Nannofossil frequency data were converted into the number of specimens per square millimeter for the evaluation of the biostratigraphic signal and into percentages to estimate the paleoecological significance of the

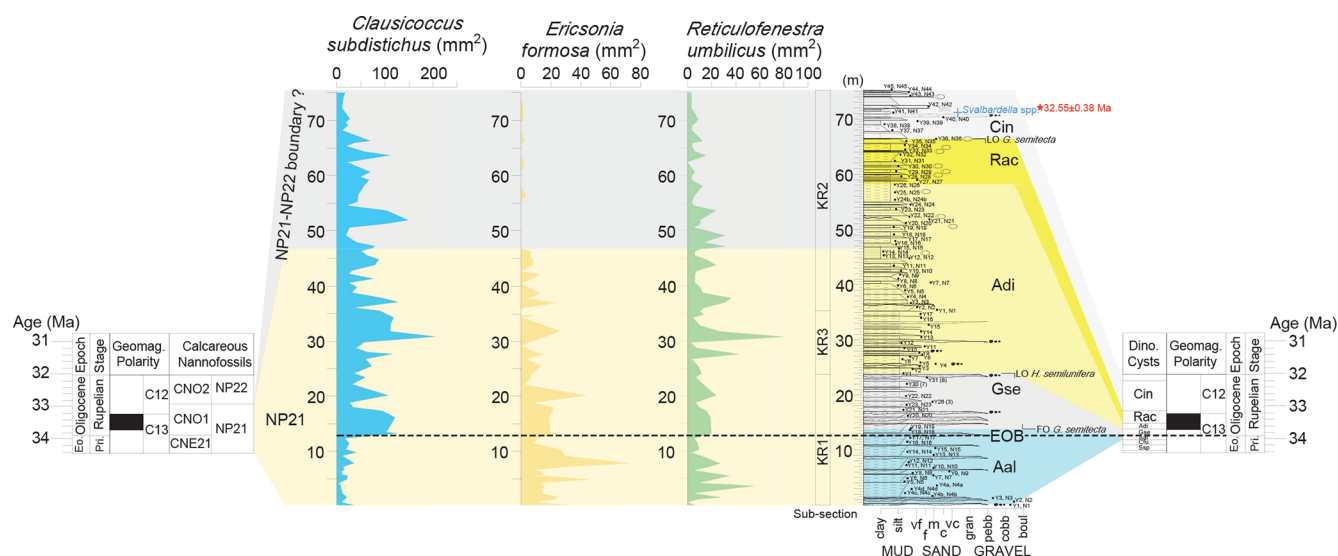


Figure 2. Stratigraphic log (in m) of the Karaburun composite section with relative abundances of marker calcareous nannofossils. KR1, KR2, and KR3 are the abbreviations for the studied subsections from the Karaburun area. The biostratigraphic (calcareous nannofossil and dinoflagellate cyst) correlations to the geological timescale (Gradstein et al., 2012) are indicated by colored shading. The red star on the log shows the level of the tuff layer (32.65 ± 0.38 Ma), while the blue cross indicates the level of sample with cold-water dinoflagellate *Svalbardella cooksoniae*, indicating a cooling event occurred during the early part of Chron C12r, near the NP21/NP22 boundary.

assemblage variations. The position of biohorizons recognized in this study is based on abundance patterns of index species, according to Agnini et al. (2014) and Viganò et al. (2023a), and are labeled as follows: top (T), the highest occurrence of a taxon, and base common and continuous (Bc) and top common and continuous (Tc), the lowest and highest common and continuous occurrence of a taxon. For calcareous nannofossil taxonomy, we refer to Perch-Nielsen (1985), Agnini et al. (2014), and the Nannotax web library (<https://www.mikrotax.org/Nannotax3>, last access: 15 December 2024). The biostratigraphic schemes adopted here are those of Martini (1971) and Agnini et al. (2014).

4.3.2 Marine palynology – dinocysts

For marine palynological analysis, emphasizing dinocysts, 42 samples were prepared at Petrostrat laboratories (Conwy, Wales, UK; sections KR1 and KR2) and another 10 (from the subsection KR3) at Utrecht University laboratories, according to typical palynological processing techniques (see, e.g., Cramwinckel et al., 2020). This involves freeze-drying and precision weighing, as well as subsequent HCl and HF treatments, followed by sieving residues over a $15 \mu\text{m}$ mesh sieve, before slides were produced for light microscopy from the residues. Samples are spiked with a known amount of *Lycopodium clavatum* spores to allow for absolute quantitative analysis (Stockmarr, 1973). After a broad palynofacies characterization (non-quantitative), light microscopical analysis included counting of broad categories of aquatic and terrestrial palynomorphs up to a minimum of 100 iden-

tifiable dinocysts per sample. Fragments of palynomorphs, whether identifiable or not (including indeterminate fragments of dinocyst remains, as well as fragments of benthic foraminiferal inner linings), were also quantified (see Table S1 in the Supplement).

For dinocyst taxonomy, we refer to that cited in Williams et al. (2019), except for taxa belonging to the Wetzelielloideae (see discussion in Bijl et al., 2017). All materials are stored in the collection of the Marine Paleooceanography and Palynology group at the Laboratory of Palaeobotany and Palynology (Utrecht University, Faculty of Geosciences).

4.4 Geochronology

U–Pb dating

A 30 cm thick volcanic tuff layer was identified at the 71.5 m level of the KR composite section, serving as a key marker for constraining the age of the deposits. A total of 3 kg of tuff material was crushed, and zircon crystals were separated by standard heavy liquid techniques and mounted in epoxy resin. Thirty-five zircon crystals were dated via U–Pb at the Envitop analytical facility at CEREGE using an Element XR ICP-MS connected to a NWR193 laser (ArF 193 nm) ablation system. Zircon crystals were ablated with a $25 \mu\text{m}$ spot diameter, a 15 Hz pulse repetition rate, an energy fluence of 1.5 J cm^{-2} , and a carrier gas flow of 0.975 L min^{-1} . Data reduction, date, and date uncertainty calculations were conducted with an in-house MATLAB script. We applied rigorous filtering based on zircon morphology, U–Pb concordance, and common Pb content to ensure the reliability

of the final age determination. The dataset was filtered for concordant grains using the concordia distance method of Vermeesch (2021), which applies isometric logratios with a discordance threshold of 10 (SI units) and a reverse discordance threshold of 5 (SI units). Details about our U–Pb dating workflow and data reduction steps are given in Licht et al. (2024). The three zircon validation reference materials used during these sessions yielded offsets around TIMS ages $< 1\%$ in most cases and $< 2\%$ otherwise. Out of the 35 analyzed zircon crystals, 12 yield concordant U–Pb ages (see Table S3). The final concordia age was calculated with concordant ages only using IsoPlotR (Vermeesch, 2018).

4.5 Geochemistry

$\delta^{18}\text{O}$ and $\delta^{13}\text{C}$ analyses

Measurements of stable oxygen ($\delta^{18}\text{O}$) and carbon ($\delta^{13}\text{C}$) isotopes on benthic foraminiferal (*Cibicidoides* spp.) and planktic foraminifera (*Turborotalia ampliapertura*) test fragments were performed at GEOMAR, Kiel, on a Thermo Scientific MAT 253 mass spectrometer with an automated Kiel IV carbonate preparation device. The isotope values were calibrated versus the NBS 19 (National Bureau of Standards) carbonate standard and the in-house carbonate standard (Standard Bremen, Solnhofen limestone). Isotope values in delta notation (δ) are reported in per mill (‰) relative to the VPDB (Vienna Pee Dee Belemnite) scale. The long-term analytical precision is 0.06‰ for $\delta^{18}\text{O}$ and 0.05‰ for $\delta^{13}\text{C}$ (1σ value). Replicate measurements were not done due to the low numbers of specimens found.

5 Results

5.1 Biostratigraphy

5.1.1 Calcareous nannofossils

So far a number of high-resolution studies on calcareous nannofossils during the EOT have been published, focusing on specific regions including high latitudes (Villa et al., 2014) and middle to low latitudes (Bordiga et al., 2015; Fioroni et al., 2015; Villa et al., 2021; Jones et al., 2019). Recently, new studies on IODP sediments have further enhanced our understanding of this critical interval in the Paleogene paleoclimate history (Raffi et al., 2024; Viganò et al., 2023a, b, 2024a). Our study contributes to the knowledge of nannofossil biostratigraphy in this interval, providing detailed documentation of the EOT under marine conditions within the Eastern Paratethyan realm (see Table S2 and Plate S6 in the Supplement).

The extinction of *D. saipanensis* defines the base of Zone NP21 (Martini, 1971), which corresponds to the base of Zone CNE21 as described by Agnini et al. (2014). This species, as well as the “rosette-shaped” *Discoaster*, is absent in the low-

est samples analyzed, indicating that its last occurrence (at 34.4 Ma) predates the studied interval.

The base of common (Bc) *Clausicoccus subdistichus* group defines the onset of Zone CNO1 of Agnini et al. (2014), which corresponds to the upper part of Zone NP21 (Martini, 1971). The increase in abundance of this informal taxonomic group represents the most reliable nannofossil bioevent to approximate the EOB across different regions (e.g., Marino and Flores, 2002; Toffanin et al., 2013; Fioroni et al., 2015; Viganò et al., 2023a). In the studied area, this event is well delineated, showing an abrupt increase in abundance from approximately 17 to over 100 specimens mm^{-2} in sample N18, ca. 13 m from the base of the studied section (Fig. 2).

The top (T) of *Ericsonia formosa* marks the base of Zone NP22 of Martini (1971) and the base of Zone CNO2 (Agnini et al., 2014). However, in the studied composite section, the precise position of this bioevent remains uncertain due to the rarity and scattered occurrence of the taxon in its final range; nevertheless, it is likely located before the end of the *C. subdistichus* acme (Fig. 2). This top of common (Tc) and continuous occurrence of the *C. subdistichus* group was positioned before the top (T) of *E. formosa* by Agnini et al. (2014) in the biozonation adopted here. However, recent studies challenge this interpretation (Viganò et al., 2023a, 2024a). In fact, recent findings suggest that the top common and continuous (Tc) of this group occurs above the top (T) of *E. formosa*, as previously reported by Backman (1987) and Catanzariti et al. (1997). The top common and continuous (Tc) of *C. subdistichus* gr., occurring early in Subchron C12r, has also been documented above the top (T) of *E. formosa* in the Pacific (Toffanin et al., 2013; Viganò et al., 2023b), the Atlantic (Bordiga et al., 2015; Viganò, 2023b), and the Indian Ocean (Fioroni et al., 2015; Villa et al., 2021; Viganò, 2023a). These studies indicate that *C. subdistichus* persists and remains common even after the T of *E. formosa*. In our dataset, the abundance of *C. subdistichus* exhibits a marked decrease (Tc) in the upper 5 m of the studied section (Fig. 2). Consequently, the T of *E. formosa* (i.e., the boundary between NP21 and NP22) should be positioned at some point prior to this bioevent. This interpretation is supported by data from dinocysts (Sect. 5.1.2), which provide a better and more precise constraint for the stratigraphic position of the upper part of the investigated section.

5.1.2 Dinocysts

Our work builds on the recent integrated study by Simmons et al. (2020) and notably that by Sancay and Bati (2020), targeting the Karaburun area and outcrops using palynological approaches, emphasizing dinocysts. Their pioneering effort, using more locations and sections, but with much lower sample resolution, now shows the need for a higher-resolution approach, particularly while considering the potential recognition of a continuous EOT interval. Therefore, here we focus

on the lower parts of the section with our higher-resolution sampling.

Unfortunately, palynomorph preservation and fragmentation varies significantly across the section, ranging from (most often) very poor to only occasionally reasonable, and always typically heavily fragmented (Table S1; note the high number of undeterminable – fragments of – specimens).

The dominant palynological components throughout the succession are organic linings of benthic foraminifera, particularly their fragments, dinocysts, pollen, and spores from terrestrial higher plants (Table S1). We also recovered several other aquatic algal taxa and acritarchs. These include representatives of, e.g., fresh to brackish water elements like *Cyclopsiella*, *Pterospermella*, and *Tasmanites* spp., besides very small (< 20 µm) psilate and skolochorate cysts (viz., “acritarchs” and other “small skolochorate cysts”) of unknown ecology. Fungal spores and fruit bodies, as well as scolecodonts, are occasionally encountered as well. In terms of palynofacies (palynodebris) composition and trends, the samples are all very similar in displaying a rich mix in mainly terrestrial plant-derived elements of varying sizes, combined with various amorphous materials. Truly opaque material is conspicuously absent. No trends or breaks are apparent from this visual, non-quantitative assessment (Table S1). Overall, these results match the findings by Sancay and Bati (2020).

Although the dinocyst assemblages are difficult to quantify because of preservation and fragmentation issues, taken together, assemblages are highly diversified throughout and essentially composed of well-known late Eocene to early Oligocene taxa (see Plates S1, S2, S3, S4, and S5). The assemblages are quite comparable to those known from other EOT sections in the larger Tethyan region, e.g., from central and northeast Italy (Brinkhuis and Biffi, 1993; Brinkhuis, 1994; Van Mourik and Brinkhuis, 2005; Houben et al., 2012; Iakovleva, 2025) to North Africa (Egypt, El Beialy et al., 2019; Tunisia, Toricelli and Biffi, 2001; and Morocco, Chekar et al., 2018; Mahboub et al., 2019; Slimani et al., 2019; Slimani and Chekar, 2023) and further to the east, e.g., the Caspian Sea region (Bati, 2015), and Armenia (Iakovleva et al., 2024). In terms of robust dinocyst-based age assessment, best-calibrated information is available from central and northeast Italy (e.g., Brinkhuis and Biffi, 1993, and follow-up studies), including a detailed zonal scheme for the EOT matched with magneto- and calcareous microfossil stratigraphies. Based on the first and last regional occurrence of *Glaphyrocysta semitecta*, the base of the Gse and the Rac/Cin zonal boundary of Brinkhuis and Biffi (1993) can be recognized in the Karaburun sections (Fig. 2, Table S1). Furthermore, based on the last occurrence of *Hemiplacophora semilunifera*, the Gse/Adi zonal boundary can be recognized as well (Fig. 2). Remarkably, the important index species *Areosphaeridium diktyoplokum* has so far not been recorded in any of the subsections with confidence, hampering the recognition of the Adi/Rac zonal boundary. This is noteworthy as elsewhere in the region the species is typically

quite abundantly present in the deposits assigned to the absolute earliest Oligocene (as defined by the extinction of the hantkeninids, planktonic foraminifera; see, e.g., Brinkhuis and Visscher, 1995; Van Mourik and Brinkhuis, 2005; and Houben et al., 2012). Yet, the recognition of the other zonal boundaries allows confident correlation to the EOT interval, matching the assignments by calcareous nannofossils throughout, and the typical benthic foraminifer $\delta^{18}\text{O}$ -EOT profile (including the Oi-1a event – cooling during the early part of Subchron C12r) discussed further below.

These correlations are here bolstered by the spot occurrence of *Svalbardella cooksoniae* in sample Y41 at 71 m assigned to the Cin Zone (Figs. 2, S5a, b, and c). This event was previously described from the central Italian EOT section within the same Cin Zone (Brinkhuis and Biffi, 1993). At high northern latitudes, this species ranges from the late Eocene way into the Oligocene (e.g., Eldrett et al., 2004). Subsequent work noted that colder episodes during the Oligocene likely induced equatorward migration of such typical high-latitude taxa (e.g., Van Simaey et al., 2005). In effect, our finding reflects the earliest of such migration pulses – an event well documented by Śliwińska and Heilmann-Clausen (2011). These authors showed that *Svalbardella cooksoniae* is consistently present in the same narrow interval calibrated to the basal Subchron C12r, close to the NP21/NP22 boundary, in many high- and mid-latitude Northern Hemisphere sections, ranging from the Greenland Sea in the north to Italy in the south. Moreover, they correlated this event to the Oi-1a oxygen isotope maximum of Pekar and Miller (1996) and Pekar et al. (2002). Another interesting finding is specimens of the acritarch *Ascostomocystis potane* in samples from the subsection KR2. Documented from the basal Rupelian type section in Belgium (Stover and Hardenbol, 1993), this further confirms the assignment to the basal Oligocene.

5.2 U–Pb dating of the tuff

A concordia plot of the dated tuff is available in Fig. S4. The tuff sample yields an early Rupelian 32.55 ± 0.38 Ma (2σ) age, based on 11 out of the 12 dated zircons. The age of the tuff layer aligns with the biostratigraphic dating, which places the top of the KR composite section within the Cin dinoflagellate cysts zone (Fig. 2).

5.3 Sequence stratigraphy

Based on lithological, sedimentological, and paleontological characteristics, we interpret the depositional environment as a shelf setting exhibiting littoral and neritic characteristics, depending on fluctuating sea levels. Our sequence stratigraphic analysis identifies 10 distinct depositional sequences within this setting (Fig. 3). The lower part of the section, up to approximately 11 m, comprises three depositional sequences (S1, S2, and S3), characterized by intercalated peb-

bly/conglomeratic layers, marls, and claystones (Fig. 3). The lowstand systems tracts (LSTs) and highstand systems tracts (HSTs) contain both pebbly/conglomeratic layers and fine-grained deposits, whereas the transgressive systems tracts (TSTs) are represented exclusively by fine-grained marls and claystones. The relatively low abundance of lagoonal dinoflagellate cysts (20 %–40 %) in this interval suggests a distal position far from the coastline. Between approximately 20 and 23 m, within sequence 5, the depositional setting represents the deepest marine conditions, marking a more distal position relative to the coastline. This interval corresponds to the TST within sequence 5.

At around 23 m, just below the last conglomeratic layer, a maximum flooding surface marks the base of the HST within sequence 5, coinciding with the highest percentage of lagoonal dinoflagellate cysts. This increase in lagoonal dinoflagellates (up to 60 %–70 %) continues into the LSTs of sequences 6 and 7, indicating a more proximal position near the coastline during the Eocene–Oligocene Glacial Maximum (EOGM).

The upper part of the section, including the early Oligocene cooling (see Sect. 6.3), consists of four sequences (S7, S8, S9, and S10). A notable difference in the thickness of the depositional sequences is observed between the lower section (up to ~11 m) and the overlying sequences (from ~11 m to the top) (Fig. 3). This variation in depositional thickness could be related to obliquity forcing during the latest Eocene – a process that has been identified in several terrestrial and marine records (e.g., Abels et al., 2011; Jovane et al., 2006; Boulila et al., 2021).

Finally, we compared our reconstructed relative sea-level variations, based on the depositional sequences and systems tracts described above, with the global sea-level reconstruction of Miller et al. (2020) (Fig. 3). In the Eastern Paratethys region, relative sea-level evolution during the latest Eocene and early Oligocene appear to follow a pattern parallel to global sea-level changes. (Note that the base of the Karaburun composite section is younger than 34.4 Ma; see Sect. 5.1.1.) This high-resolution sea-level evolution offers a refined reconstruction of Eastern Paratethys sea-level changes (e.g., Popov et al., 2010) and provides a valuable framework for future studies to further reveal the history of Paratethys sea-level evolution.

5.4 Geochemistry

5.4.1 $\delta^{18}\text{O}$ and $\delta^{13}\text{C}$ isotope analyses

The $\delta^{18}\text{O}$ values of benthic foraminifera (*Cibicidoides* spp.) in the Karaburun composite section range from -9.5‰ to 1.0‰ , displaying distinct temporal variations throughout the sequence. At the base of the section, at 11.40 m, just before the EOB, a small positive peak (1.0‰) is noticeable (Fig. 4). Following this, a pronounced and abrupt negative shift from -0.1‰ to -9.5‰ is evident just after the

Eocene–Oligocene Boundary (EOB). Following the abrupt negative shift, the $\delta^{18}\text{O}$ values increase gradually and then sharply, reaching a peak of 1.0‰ at 19.60 m. This represents a two-phase increase in $\delta^{18}\text{O}$ during the EOT as in other EOT records (e.g., Katz et al., 2008), but with a negative shift in between. Following the second increase, a negative shift to -2.3‰ occurs at 22 m, followed by a renewed increase in $\delta^{18}\text{O}$ values, forming a plateau that culminates at 0.6‰ by 36.75 m. The $\delta^{18}\text{O}$ values then decline, reaching a negative peak of -1.6‰ at 40.25 m, before gradually rising to 0.4‰ at 60 m, marking a second, shorter plateau. This plateau is interrupted by a decrease to -1.6‰ at 65.75 m, followed by a slight recovery to 0.5‰ at 69 m. In the uppermost portion of the section, $\delta^{18}\text{O}$ values drop to -2.4‰ at 74.50 m and then exhibit a modest increase toward the top of the section (Fig. 4).

The $\delta^{13}\text{C}$ values of benthic foraminifera (*Cibicidoides* spp.) in the Karaburun composite section range from -0.7‰ to 2.2‰ , exhibiting greater variability compared to the $\delta^{18}\text{O}$ values. However, similar to the $\delta^{18}\text{O}$ values, the $\delta^{13}\text{C}$ values also display a prominent shift towards more depleted levels (from 2.1‰ to 0‰) just after the EOB (Fig. 5). The two-phase increase in $\delta^{13}\text{C}$ (from the EOB up to ca. 24 m) is again evident, interrupted by a sharp decline (ca. 20 m) that corresponds precisely with changes in $\delta^{18}\text{O}$ (Figs. 4 and 5). The $\delta^{13}\text{C}$ appears to lag behind by several tens of thousands of years compared to the two-phase increase in $\delta^{18}\text{O}$ (e.g., Coxall and Wilson, 2011). The increase just before the EOB between 11.20 and 12 m represents a 1.3‰ shift, followed by a 1.5‰ increase between 13.20 and 15 m and a 1.0‰ increase between 19.60 and 23 m. Before the EOB, two more major positive carbon isotope excursions are observed at the base of the section: one between 1 and 7.5 m (1.0‰) and the second between 7.5 and 11.20 m (0.1‰). All excursions, except the second at the base (between 7.5 and 11.20 m), exhibit a significant positive shift of $\geq 1.0\text{‰}$. After the excursion between 19.60 and 23 m, the $\delta^{13}\text{C}$ values drop sharply (around 23–27 m) before exhibiting another series of positive carbon isotope excursions in the middle and upper parts of the section (Fig. 5). Like the excursions at the base of the section, the excursions in the middle and upper parts also display positive shifts of approximately 1‰ , with the most pronounced reaching 1.5‰ . This pattern reflects a dynamic carbon cycle with notable variations throughout the sequence.

Due to the intermittent presence of the planktic foraminifera *Turborotalia ampliapertura* along the composite section, the $\delta^{18}\text{O}$ and $\delta^{13}\text{C}$ records of planktic foraminifera exhibit some gaps (Figs. 6 and S1 in the Supplement). Nevertheless, the overall trends and shifts remain discernible. Similar to the $\delta^{18}\text{O}$ record of benthic foraminifera, the $\delta^{18}\text{O}$ of planktic foraminifera exhibits a clear positive shift at the base of the section at 11.40 m just before the EOB, albeit slightly smaller (1.2‰). Following a slight positive shift (0.4‰) just after the EOB at 14.45 m, the most prominent and significant positive shift recorded by the benthic

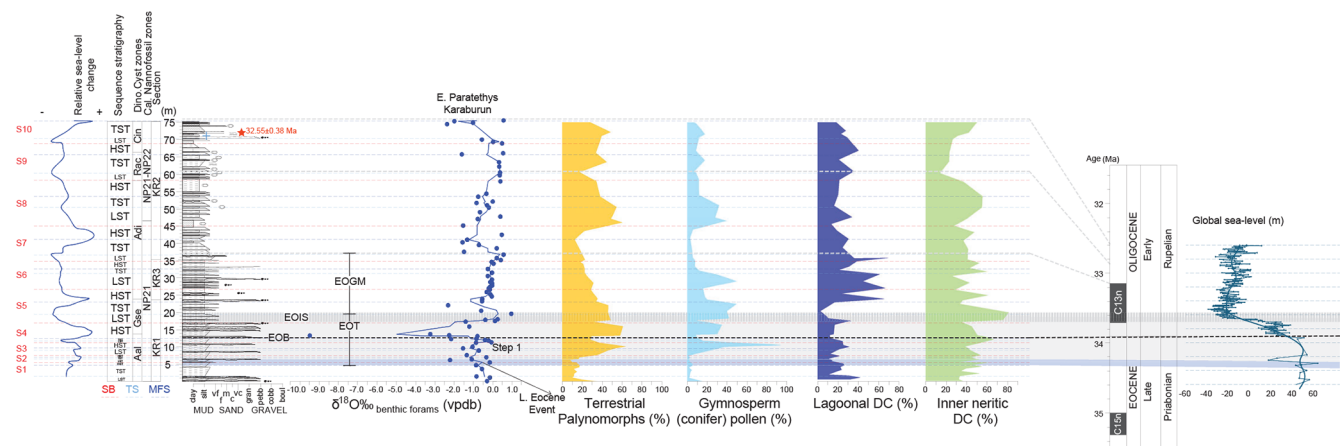


Figure 3. Stratigraphic log (in m) of the Karaburun composite section showing sequence stratigraphic interpretations and reconstructed relative sea level. The sequence stratigraphic interpretation and the reconstructed relative sea-level changes are based on the analysis of benthic foraminifera $\delta^{18}\text{O}$ values, along with the abundance of terrestrial palynomorphs and lagoonal and inner neritic dinocysts. The red star shows the level of the tuff layer on the log, while the blue cross indicates the level of sample with the cold-water dinocyst *Svalbardella cooksoniae*. Correlation to the reconstructed global sea-level curve (Miller et al., 2020) and to the geological timescale (Gradstein et al., 2012) could be seen on the right side. S: sequence; SB: sequence boundary; TS: transgressive surface; MFS: maximum flooding surface; LST: lowstand systems tract; TST: transgressive systems tract; HTS: highstand systems tract; EOB: Eocene–Oligocene Boundary; EOT: Eocene–Oligocene Transition; EOIS: Earliest Oligocene Oxygen Isotope Step; EOGM: Early Oligocene Glacial Maximum.

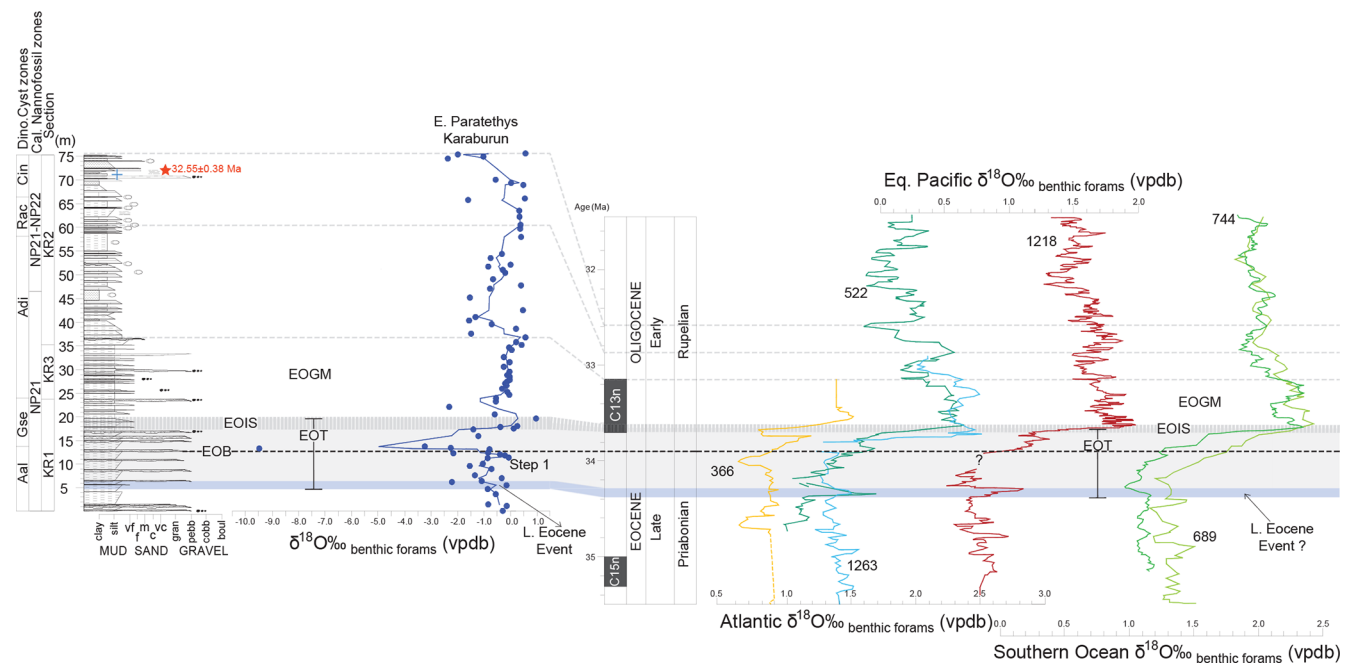


Figure 4. The stratigraphic log (in m) of the Karaburun composite section including the results of benthic foraminifera $\delta^{18}\text{O}$ record (blue dots and line showing three-point running mean), highlighting the chronostratigraphic characteristics of the Eocene–Oligocene Transition (EOT). Apparent correlations were established by aligning the Karaburun data with high-resolution deep-sea benthic foraminifera $\delta^{18}\text{O}$ records from the South Atlantic sites 522 (Zachos et al., 1996) and 1263 (Langton et al., 2016) and compared to the tropical Atlantic site 366 (Langton et al., 2016), the Southern Ocean sites 744 and 689 (Zachos et al., 1996; Diester-Haass and Zahn, 1996), and the equatorial Pacific site 1218 (Coxall and Wilson, 2011). Key features in the $\delta^{18}\text{O}$ records, such as positive and negative shifts and their amplitudes, were used to define EOT characteristics, including the Late Eocene Event, the Earliest Oligocene Oxygen Isotope Step (EOIS), and the Early Oligocene Glacial Maximum (EOGM). The Eocene–Oligocene Boundary (EOB) was identified through biostratigraphic analyses (see Sect. 5.1). The red star on the log marks the tuff layer, while the blue cross indicates the occurrence of the cold-water dinocyst *Svalbardella cooksoniae*.

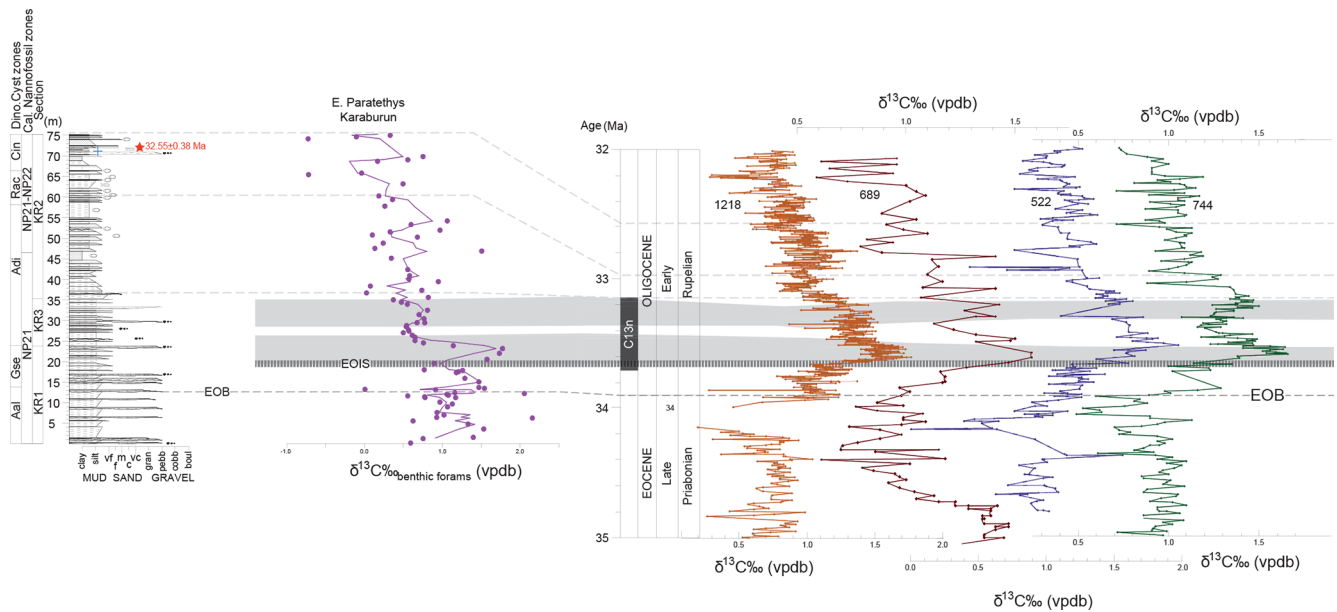


Figure 5. Benthic foraminifera $\delta^{13}\text{C}$ record (pink dots and line showing three-point running mean) of the Karaburun composite section along the stratigraphic log (in m) highlighting the chronostratigraphic features of the Eocene–Oligocene Transition (EOT). Correlations were made with deep marine records from site 689 in the sub-Antarctic Atlantic (Diester-Haass and Zahn, 1996), site 1218 in the equatorial Pacific (Coxall and Wilson, 2011), site 522 in the South Atlantic (Zachos et al., 1996), and site 744 in the Southern Ocean (Zachos et al., 1996). Alignment of high-resolution benthic foraminifera $\delta^{13}\text{C}$ records from these sites with the Karaburun data revealed a corresponding double-peak isotope feature (gray shading) after the Earliest Oligocene Oxygen Isotope Step (EOIS) within the Early Oligocene Glacial Maximum (EOGM). The Eocene–Oligocene Boundary (EOB) was determined through biostratigraphic analysis (see Sect. 5.1). The red star marks the tuff layer, while the blue cross indicates the level of sample containing the cold-water dinocyst *Svalbardella cooksoniae*.

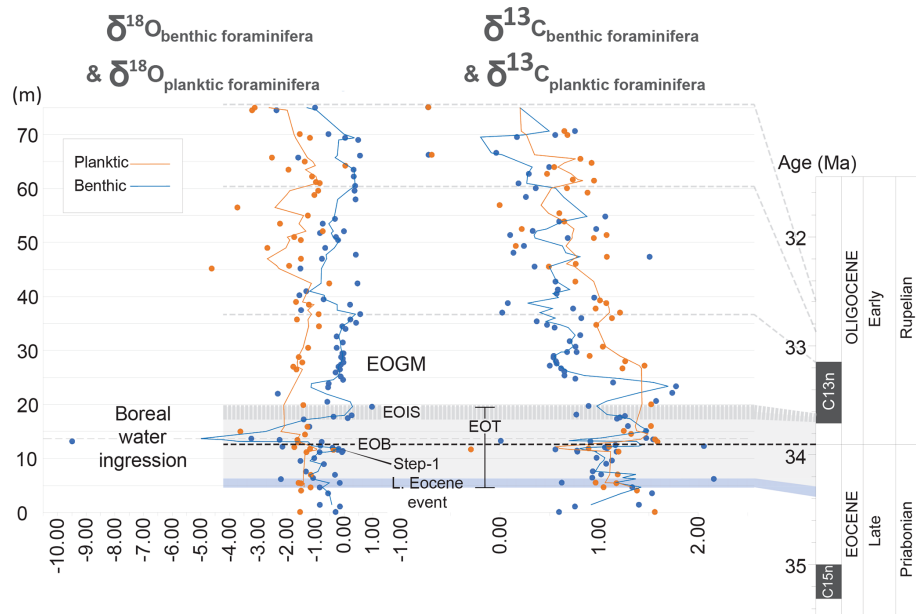


Figure 6. Oxygen ($\delta^{18}\text{O}$) and carbon ($\delta^{13}\text{C}$) stable isotope values for the benthic and planktic foraminifera from the Karaburun composite section. The black dashed line represents the level for the boreal water ingress just after the Eocene–Oligocene Boundary (EOB). EOT: Eocene–Oligocene Transition. EOIS: Earliest Oligocene Oxygen Isotope Step. EOGM: Early Oligocene Glacial Maximum.

foraminifera is not fully captured in the planktic foraminifera record due to the absence of *T. ampliapertura* in the 4 m interval between 15.90 and 19.90 m. However, the positive 2.3‰ shift observed from 15.90 to 19.90 m represents partly the major positive shift, albeit smaller than the shift recorded in the benthic foraminifera $\delta^{18}\text{O}$. An interval of ca. 7 m without any *T. ampliapertura* follows the pronounced positive shift between 19.90 and 26.5 m, obscuring the $\delta^{18}\text{O}$ record for that interval. Following the barren interval, a gradual increase of 0.9‰ is clearly observed, extending up to 36.75 m. In the interval between 36.75 and 61 m, the $\delta^{18}\text{O}$ record of planktic foraminifera fluctuates, exhibiting two significant alternating trends of decrease and increase. Following this fluctuation, a gradual decrease is observed at the top of the section, followed by a sharp decline.

A distinct decline in the $\delta^{13}\text{C}$ record of planktic foraminifera (1.5‰) is observed just before the EOB at 11.60 m (Figs. 6 and S2). Following this decline, $\delta^{13}\text{C}$ values increase at the EOB, reaching up to 1.5‰ at 15.90 m with a shift of 1.8‰. Due to the infrequent presence of *T. ampliapertura*, the interval between 15.90 and 26.5 m is not fully represented; however, this interval includes the highest $\delta^{13}\text{C}$ values observed. After these peak values, a gradual decrease is noted towards the top of the section, with six positive shifts interrupting this trend: between 34.50 and 36.75, 45.20 and 47, 49 and 51, 56.50 and 61, 62.25 and 65.75, and 65.75 and 70.10 m. At the top of the section, a sharp decline in $\delta^{13}\text{C}$ values is noticeable.

5.5 Paleoenvironment and paleoecology

5.5.1 Calcareous nannofossils

Calcareous nannoplankton are highly sensitive to environmental changes in their surface water habitats, and fluctuations in nannofossil assemblages are interpreted as responses to shifts in sea surface temperature (SST), nutrient concentrations, salinity, and other environmental factors (e.g., Aubry, 1992; Winter and Siesser, 1994), thereby reflecting paleoceanographic perturbations. Numerous studies have explored the ecological tolerance of extinct taxa, establishing paleoecological preferences through biogeographic studies (e.g., Wei and Wise, 1990) and comparison with diverse environmental proxies (e.g., Villa et al., 2014). We discuss the behavior of several taxa within the Karaburun assemblage, based on paleoecological affinities outlined in previous works.

Reticulofenestra daviesii and *Chiasmolithus* spp. are considered cool-water taxa (Wei et al., 1992; Villa et al., 2008) with a preference for eutrophic conditions (Villa et al., 2014; Viganò et al., 2024b). This paleoecologic group is recorded with very low relative abundances, with few positive peaks in the middle part of the studied section. *Cyclicargolithus floridanus*, a typical eutrophic open-ocean species (Auer et al., 2014), occurs with abundances reaching up to 50 % in the lower and upper part of the studied section, sug-

gesting high-productivity conditions (Aubry, 1992; Dunkley Jones et al., 2008; Villa et al., 2021) (Fig. S3). Small reticulofenestrads constitute a significant component of the assemblages, reaching over 60 % in the middle part of the section. They have been reported as dominant components of the nannoflora along continental margins (Haq, 1980). These settings are typically characterized by eutrophic conditions, driven by continental runoff and/or riverine input. Consequently, these small coccoliths are regarded as opportunistic taxa with broad ecological tolerance, yet particularly well adapted to nutrient-rich environments (Aubry, 1992) and indicative of increased availability of terrigenous nutrient (Wade and Bown, 2006).

The genus *Helicosphaera* has been linked to increased nutrient availability (De Kaenel and Villa, 1996; Ziveri et al., 2004). Studies on extant coccolithophorids confirm the relationship of helicosphaerids with high primary productivity rates (Haidar and Thierstein, 2001; Toledo et al., 2007) and their preference for near-shore environments (Ziveri et al., 2004; Guerreiro et al., 2005). At the Karaburun section, this genus is recorded at low abundances but occurs consistently throughout the section (Fig. S3).

Evidence of nutrient availability is further supported by the presence of braarudosphaerids, which are associated with coastal, low-salinity waters (Peleo-Alampay et al., 1999; Thierstein et al., 2004; Konno et al., 2007), eutrophic conditions (Cunha and Shimabukuro, 1997; Bartol et al., 2008), and the influx of terrigenous material (Švábenická, 1999). Braarudosphaerids are rarely found in the open ocean and thrive under unusual marine conditions, demonstrating a tolerance for environmentally stressed settings. Similar conditions are indicated by the presence of *Micrantholitus*, a taxon typically associated with shallow marine environments (Bown, 2005), reduced salinity, and eutrophic conditions (Street and Bown, 2000; Bown and Pearson, 2009). These penthaliths occur from the base of the investigated section, albeit at low percentages and with a discontinuous distribution, further suggesting eutrophication and reduced salinity (Fig. S3).

The presence of Ascidian spicules, with their highest and continuous occurrence in the middle–upper part of the section, also points to a shallow marine depositional setting (e.g., Varol, 2006; Ferreira et al., 2019) and high surface water productivity (Toledo et al., 2007). Furthermore, the relatively common occurrence of holococcoliths (mainly *Lanternithus minutus* and *Zigrablithus bijugatus*), *Pontosphaera* spp., and *Helicosphaera* spp., taxa prone to dissolution (Bown, 2005; Monechi et al., 2000), reinforces the interpretation of a shallow-water environment.

5.5.2 Marine palynology – dinocysts

For the analysis of the marine palynological assemblages, emphasizing dinocysts, we rely on the taxonomical and ecological dinocyst groups derived from modern distribu-

tions (e.g., Zonneveld et al., 2013; Marret and De Vernal, 2024) and empirically based paleoecological information or the Paleogene dinocysts following previous works (e.g., Brinkhuis, 1994; Pross and Brinkhuis, 2005; Sluijs et al., 2005; Frieling and Sluijs, 2018). However, as mentioned above, the assemblages are generally too poorly preserved to allow for detailed quantitative considerations. Yet, the overall quantitative characteristics of the studied samples, including significant terrestrial input and the consistent dominance of taxa typically associated with restricted marine to inner neritic environments (e.g., the goniodomid group such as *Homotryblum*, *Polysphaeridium*, *Heteraulacacysta*, *Eocladopyxis* spp.) and peridinoid cysts (*Lentinia*, *Phthanoperidinium*, *Senegalinium*, *Deflandrea* spp.), as well as neritic to outer neritic forms (e.g., *Areoligera*, *Glaphyrocysta*, *Enneadocysta*, *Spiniferites*, *Operculodinium* spp.), together with a minor yet persistent presence of oceanic taxa like *Impagidinium* and *Nematosphaeropsis* spp. suggest deposition in an open marine, hemipelagic setting, comparable to central Italian sections (cf. Brinkhuis and Biffi, 1993).

Despite the issues with preservation throughout, a percentage plot of freshwater-tolerant and restricted to inner neritic marine taxa vs. more offshore taxa still reveals stronger influxes in the latter part of the Gse and within the Adi Zone (Table S1; see above and compare, e.g., Frieling and Sluijs, 2018; Sluijs and Brinkhuis, 2024). In effect, this aspect matches the records from elsewhere (e.g., the Italian sections) and was previously interpreted to reflect general eustatic sea level lowering associated with the Oi-1 stable isotope event reflecting the earliest glaciation of Antarctica (e.g., Brinkhuis, 1994). In terms of temperature/climatic changes, the conspicuous increase in Gymnospermous (conifer) bisaccate pollen input may be significant as well. Again, a similar trend was noted in the Italian sections across the EOT (Brinkhuis and Biffi, 1993; Brinkhuis, 1994).

6 Discussion

6.1 Age control overview

An initial age model for the KR composite section was constructed using tie points derived from nannofossil and dinocyst biozonations, combined with U–Pb dating of a tuff layer at 71.5 m (Fig. 2). Additional age constraints were obtained by aligning the Karaburun benthic foraminifera $\delta^{18}\text{O}$ data with the high-resolution benthic foraminifera $\delta^{18}\text{O}$ record from the Atlantic sites 522 and 1263 (Fig. 4). This alignment was achieved by identifying corresponding features in the isotope records, such as positive and negative shifts and their amplitudes. The carbon isotope record of benthic foraminifera provided independent validation of this tuning (Fig. 5). The $\delta^{13}\text{C}$ benthic foraminifera data from the Karaburun area were correlated and aligned with global high-resolution benthic foraminifera $\delta^{13}\text{C}$ records from deep-sea sites, including 1218 (equatorial Pacific), 689 (sub-

Antarctic Atlantic), 522 (South Atlantic), and 744 (southern Indian Ocean). Similarly, the planktic foraminifera provided a further confirmation for our age model (Figs. S1, S2). The planktic foraminifera $\delta^{18}\text{O}$ and $\delta^{13}\text{C}$ data from the Karaburun area were correlated and aligned with high-resolution $\delta^{18}\text{O}$ and $\delta^{13}\text{C}$ records of planktic foraminifera in hemipelagic sediment cores retrieved from the African margin of the Indian Ocean (Tanzania Drilling Project sites 12 and 17, Pearson et al., 2008). All ages were assigned following the integrated magneto-biostratigraphic GTS2012 timescale. Our geochemical results indicate that the increases in $\delta^{18}\text{O}$ and $\delta^{13}\text{C}$ observed during the EOT at mid- and high-latitude sites in the South Atlantic, Southern Ocean, and Pacific are also present in the Paratethys, verifying that these signals are genuinely global and valuable for stratigraphic correlation.

According to the constructed age model, the base of the section dates to the late Eocene (late Priabonian). The EOB is identified at 12.75 m. The middle and upper parts of the composite KR section correspond to the early Oligocene (early Rupelian) (Fig. 2). The revised age constraints established in this study offer a robust chronostratigraphic framework for the latest Eocene to early Oligocene interval of the Karaburun section, surpassing the accuracy of prior studies (e.g., Less et al., 2011; Okay et al., 2019; Simmons et al., 2020). However, we have to note that the absence of the typically abundant index taxon *Areosphaeridium diktyoplokum* in all studied subsections currently hampers precise recognition of the Adi/Rac zonal boundary and may reflect local paleoenvironmental or taphonomic conditions or, alternatively, point to a slight stratigraphic gap or condensed interval – a possibility that merits further investigation.

6.2 The EOT

At the deep Atlantic site 522 and Pacific site 1218, the Late Eocene Event is marked by a transient interval of positive $\delta^{18}\text{O}$ values, reflecting a short-lived cooling or glacial episode (Hutchinson et al., 2021) (Fig. 4). This isotopic shift measures approximately 0.6‰ and 0.4‰ at site 522 and site 1218, respectively. Similarly, the base of the KR composite section exhibits an increase of 0.7‰ in benthic foraminifera $\delta^{18}\text{O}$ values at approximately 5.5 m, which we interpret as evidence of the Late Eocene Event (Fig. 4). The onset of this event coincides with the extinction of *Discoaster saipanensis* at 34.44 Ma at site 1218. Based on calcareous nannofossil data (i.e., the absence of *D. saipanensis*), the base of the KR section is inferred to be younger than 34.44 Ma, supporting this correlation. The Late Eocene Event represented by this 0.7‰ positive shift in $\delta^{18}\text{O}$ values at approximately 5.5 m marks the onset of the EOT in the KR composite section (e.g., Hutchinson et al., 2021) (Fig. 4).

The initial $\delta^{18}\text{O}$ step increase, occurring just before the EOB, has been identified as step 1 in some records (e.g., EOT-1 in Katz et al., 2008; Precursor Glaciation in Scher et

al., 2011). The first 1.0‰ $\delta^{18}\text{O}$ increase observed in the KR composite section at 11.40 m is interpreted as step 1 as in the previous records (e.g., EOT-1 in Katz et al., 2008; Precursor Glaciation in Scher et al., 2011) (Fig. 4). A similar $\delta^{18}\text{O}$ increase of 0.9‰ is recorded in the Alabama St. Stephens Quarry core (Miller et al., 2008). The onset of step 1 is dated to 34.15 Ma, with an estimated duration of approximately 40 kyr (Hutchinson et al., 2021).

The Earliest Oligocene Oxygen Isotope Step (EOIS) represents a rapid $\delta^{18}\text{O}$ increase (0.7‰ or more) occurring well after the EOB, within the lower part of Chron C13n (Hutchinson et al., 2021). The peak $\delta^{18}\text{O}$ is recorded at approximately 33.65 Ma, with the entire EOIS lasting around 40 kyr. In the KR composite section, the positive shift associated with EOIS is approximately 2‰, peaking at 1‰ at 19.60 m, marking the end of the EOT (Hutchinson et al., 2021) (Fig. 4).

The Early Oligocene Glacial Maximum (EOGM) is characterized as a prolonged period of cold climate and glaciation during the early Oligocene, corresponding to the most of paleomagnetic Subchron C13n (Hutchinson et al., 2021) (Fig. 4). It spans from approximately 33.65 to 33.16 Ma, lasting about 490 kyr. Correlation between the Karaburun data and global deep-sea records was achieved by aligning the peak-to-peak $\delta^{18}\text{O}$ stratigraphic intervals, starting at the top of the EOIS at 19.60 m and extending to another peak at 36.75 m (0.6‰) corresponding to the top of Subchron C13n (Fig. 4).

Overall, the $\delta^{18}\text{O}$ record of benthic foraminifera from the Karaburun composite section closely mirrors global $\delta^{18}\text{O}$ trends from deep-sea sites, except for a sharp decrease observed just after the EOB (Fig. 4). The EOT signal is clearly recorded in the $\delta^{18}\text{O}$ benthic foraminifera data from the Karaburun composite section. However, the relatively lower $\delta^{18}\text{O}$ values and sharp decrease just after the EOB are attributed to regional conditions in the Paratethys Sea, as discussed in Sect. 6.4.

6.3 The early Oligocene cooling

The presence of the cold-water dinoflagellate *Svalbardella cooksoniae* within a brief interval of the early Oligocene in the North Atlantic and Western Neo-Tethyan realms has been previously documented and linked to the Oi-1a oxygen isotope maximum (Śliwińska and Heilmann-Clausen, 2011). This oxygen isotope maximum representing a cooling event occurs during the early part of Subchron C12r, near the NP21/NP22 boundary. In the KR composite section, the *Svalbardella cooksoniae*-bearing sample aligns with an oxygen isotope maximum at approximately 71 m, occurring during the early phase of Subchron C12r (Fig. 4). Consequently, the boundary between NP21 and NP22 is likely located near this level. In the North Sea, the *S. cooksoniae* event was identified at the top of the regressive systems tract (OSS-21 RST) in the 11/10-1 well (Śliwińska, 2019). Simi-

larly, in the KR composite section, the *S. cooksoniae* event is positioned at the top of a lowstand systems tract, in agreement with the North Sea data (Fig. 3). Strontium isotope analyses by Jarsve et al. (2015) suggest an age of 32.66 Ma for this event. Our U–Pb dating of the tuff layer located just above the *Svalbardella* spp.-bearing interval yields an age of 32.55 ± 0.38 Ma, aligning closely with the strontium-based age reported by Jarsve et al. (2015). These findings further support the interpretation of Śliwińska and Heilmann-Clausen (2011) that the earliest Rupelian *S. cooksoniae* interval across the Tethys, Central Europe, the North Sea Basin, the Norwegian–Greenland Sea, and the Eastern Paratethys is coeval with the Oi-1a event and corresponds to a significant sea-level fall (Fig. 3).

In support of the geochemical evidence provided by $\delta^{18}\text{O}$ values in benthic foraminifera, a notable increase in gymnospermous (conifer) bisaccate pollen is clearly observed at the KR composite section during the EOT, EOGM, and Oi-1a events (Fig. 3). This increase is likely associated with cooling and glaciation events occurring during these intervals, as previously suggested by Brinkhuis and Biffi (1993) and Brinkhuis (1994).

The early Oligocene cooling event (Oi-1a) was previously dated to 32.8 Ma by Pekar et al. (2002). At the KR composite section, the peak $\delta^{18}\text{O}$ values in benthic foraminifera (~ 0.4 ‰) observed around 58–60 m are interpreted as representing the Oi-1a event. Our age model corroborates the age proposed by Pekar et al. (2002), further supporting a timing of 32.8 Ma for these peak values.

6.4 The regional and global effects in the Paratethys

The benthic foraminiferal oxygen and carbon isotope records from the Karaburun area closely resemble deep-sea records from Atlantic sites 522 and 1263 during the latest Eocene and early Oligocene (Figs. 4, 5). However, a notable distinction is the pronounced negative $\delta^{18}\text{O}$ shift just after the EOB – a feature characteristic of the Paratethys region (Figs. 4 and 7) which will be discussed in the following. Firstly, it is noticeable that the overall benthic and planktic foraminifera $\delta^{18}\text{O}$ values are more depleted than global records from the EOT. These depleted values likely reflect a regional effect rather than diagenetic alteration, as the exceptional preservation and glassy appearance of the foraminiferal shells from the KR composite section and other Paratethys sites (e.g., Ozsvárt et al., 2016) suggest minimal recrystallization. A major diagenetic overprint affecting the entire basin is also improbable given the differing tectonic and depositional histories across the Paratethys subbasins. Additionally, the observed timescale (< 100 ka) and the significant magnitude of changes in proxy records from the Paratethys Basin are unlikely to be explained by regional tectonic processes. Instead, factors such as basin restriction, enhanced precipitation, and/or freshwater input due to increased runoff or changing hydrological conditions during the EOT seem more

plausible explanations. Similar $\delta^{18}\text{O}$ depletion has been documented in other marginal basins during the EOT (e.g., Pearson et al., 2008; De Lira Mota et al., 2023), further supporting a localized effect in semi-restricted environments due to local hydrology and climate. Indeed, these values are consistent with the isotopic composition of meteoric waters at mid-latitude coastal regions ($\delta^{18}\text{O} \sim -5\text{‰}$ to -10‰ ; Dansgaard, 1964; Gat, 1996). During the Rupelian (35–31 Ma), the dominant influence of Atlantic-derived westerlies likely brought increased precipitation with a depleted $\delta^{18}\text{O}$ signature to the Western and Central Paratethys. This interpretation was supported by $\delta^{18}\text{OPO}_4$ values from herbivore tooth enamel, which reflect the depleted isotopic composition of drinking water (Kocsis et al., 2014). The enhanced precipitation was likely due to the intensification of the westerlies and the reorganization of oceanic and atmospheric circulation (e.g., Hou et al., 2022). As global cooling progressed and the meridional temperature gradient steepened, the westerlies strengthened, enhancing vapor transport from the Atlantic into Eurasia, contributing to higher precipitation in the Western and Central Paratethys (e.g., Kocsis et al., 2014; Li et al., 2018). Modeling studies further suggest prevailing westerly winds during winter at middle to high latitudes in the Rupelian (Li et al., 2018). The “continental effect”, where $\delta^{18}\text{O}$ in meteoric water becomes progressively fractionated with increasing transport distance from the Atlantic, likely contributed to more negative $\delta^{18}\text{O}$ values in the Karaburun area (e.g., Kocsis et al., 2014). Basin geometry, particularly water depth, plays a crucial role in evaporation dynamics within a semi-isolated system like the Paratethys. The Western Paratethys, characterized by deeper basins, had a higher heat capacity and greater thermal inertia, leading to moderated surface temperatures and lower evaporation rates. In contrast, the shallower Eastern Paratethys had lower heat capacity, allowing for rapid surface warming, especially in warmer seasons, which enhanced evaporation. Additionally, wind-driven effects likely played a significant role. In deeper basins, wind-driven mixing redistributed heat within the water column, reducing extreme surface warming and stabilizing evaporation rates. In shallower areas, reduced mixing allowed surface waters to remain warmer, leading to increased evaporation, particularly under strong seasonal winds. Hence, further east, evaporation over the shallower Eastern Paratethys may have added moisture to westerly air trajectories, resulting in relatively less negative $\delta^{18}\text{O}$ values in the Northern Caucasus (Karaburun, Belaya and Chirkei sections in Fig. 7) and increased inland precipitation (Fig. 7). A similar precipitation gradient, with wetter conditions in the Western–Central Paratethys and drier conditions in the east, is also evident in an Oligocene climate reconstruction based on plant macrofossil data (Li et al., 2018). Additionally, the increased freshwater input in the Paratethys at the EOB could be plausibly explained by the major sea-level fall and falling base level, driven by glacio-eustasy associated with the growth of Antarctic ice sheets during the EOT. The

reorganization of rivers due to the falling base level would have introduced fresh water into the depositional epicenters of the Paratethys. Combined, the effects of regional hydrological change and the base level fall due to the global major sea-level fall at the EOB might have resulted in the depleted $\delta^{18}\text{O}$ values observed in the Paratethys. Despite the localized variations in the depletion of $\delta^{18}\text{O}$ values, the relatively consistent $\delta^{18}\text{O}$ depletion observed across Paratethys sections suggests a uniform basin-wide isotopic background. This consistency allows for reliable identification of major trends and isotopic excursions in the Paratethys Basin during the EOT.

Secondly, it is noticeable that before the EOB a parallel trend could be observed for the benthic and planktic foraminifera $\delta^{18}\text{O}$ and $\delta^{13}\text{C}$ values (Fig. 6). Particularly during step 1, the same trends in isotopic shifts could be clearly recognized. Most significantly, just after the EOB a distinct contrasting trend between benthic and planktic foraminifera $\delta^{18}\text{O}$ and $\delta^{13}\text{C}$ could be noticed (Fig. 6). These contrasting trends between benthic and planktic foraminifera $\delta^{18}\text{O}$ and $\delta^{13}\text{C}$ just after the EOB suggest significant stratification and a reduction in vertical mixing. The pronounced negative $\delta^{18}\text{O}$ shift in benthic foraminifera likely reflects a significant influx of isotopically light cold freshwater into the bottom waters. The slight increase in planktic foraminifera $\delta^{18}\text{O}$ at the same time suggest that the surface waters might have become relatively saline due to evaporation exceeding freshwater input in the surface layer, which would increase $\delta^{18}\text{O}$ values. Cold, freshwater inflow might have been funneled into deeper areas of the basin, displacing or mixing with bottom waters. This might have happened through the submarine channels providing sediment-laden freshwater as underflows into the deep marine turbiditic systems. However, this would have required an anti-estuarine circulation model where marine saltwater flows upstream and overrides the freshwater inflow. Indeed, an anti-estuarine circulation model for the early Oligocene Paratethys was proposed previously (Dohmann, 1991) and was later supported by Schulz et al. (2005), showing also increasing surface salinities due to evaporation of marine water based on increasing di-/tri-MTTC ratios. An early anti-estuarine circulation model for the Paratethys aligns perfectly with our abovementioned stable isotope data. The deep freshwater input could be explained by the early evolution of the Paratethys (e.g., Schulz et al., 2005). Early evolution of the Paratethys was mainly controlled by narrowing seaways connecting it to the Tethys Ocean, which led to ingressions of cold boreal water from the north (through Polish straits), initially as undercurrents (generating an anti-estuarine circulation) into the Eastern Paratethys first and then to the Central and Western Paratethys (e.g., Schulz et al., 2005; Soták, 2010). In parallel to the $\delta^{18}\text{O}$ values, a divergent trend could be observed between the benthic and planktic $\delta^{13}\text{C}$ values just after the EOB where benthic $\delta^{13}\text{C}$ declines largely, whereas the planktic $\delta^{13}\text{C}$ shows an increase (Fig. 6). In addition to the

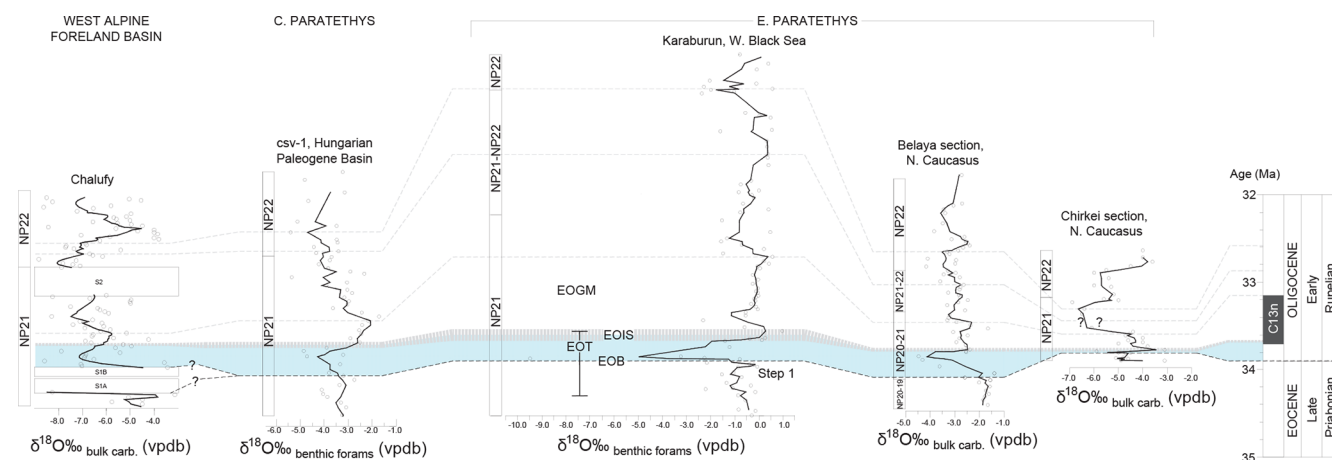


Figure 7. Oxygen stable isotope ($\delta^{18}\text{O}$) values and the characteristic negative $\delta^{18}\text{O}$ shift during the EOT observed in various Paratethys marine records. Correlations highlight the interval (light-blue shading) between the Eocene–Oligocene Boundary (EOB) and the Earliest Oligocene Oxygen Isotope Step (EOIS, gray dashed line) across various sections, including the Chalufy section in the western Alpine foreland basin, which links the Western Paratethys to the Mediterranean Tethys (Soutter et al., 2022); the csv-1 core from the Hungarian Paleogene Basin (Ozsvárt et al., 2016); the Karaburun section (this study); and the Belaya (van der Boon et al., 2019) and Chirkei (Gavrilov et al., 2017) sections from the Northern Caucasus. To account for varying sample resolutions, a three-point running mean filter was applied uniformly to all sites.

boreal freshwater ingressions, enhanced organic matter production due to increased nutrient input and then the subsequent decomposition in the isolated, stratified Paratethys waters might have released light carbon into the bottom waters. Increased $\delta^{13}\text{C}$ in planktic foraminifera could have resulted from elevated primary productivity driven by increased nutrient input, which preferentially removes isotopically light carbon from surface waters during photosynthesis, leaving the remaining carbon pool enriched in heavier carbon.

Initial boreal freshwater input by undercurrents then changes into ingressions of freshwater runoff as overflowing currents, diluting the former Paratethyan seawater (i.e., a change into estuarine circulation) (e.g., Schulz et al., 2005; Soták, 2010). This later ingressions of overflowing freshwater runoff is likely due to an enhanced precipitation and is represented as declining planktic foraminifera $\delta^{18}\text{O}$ and $\delta^{13}\text{C}$ values at ca. 15 m (Fig. 6). The $\delta^{18}\text{O}$ benthic foraminifera shows an increase during this time, which is likely related to the cooling of the bottom waters, whereas $\delta^{13}\text{C}$ of benthic foraminifera shows a positive peak suggesting an enhanced organic carbon burial. The ingressions of freshwater runoff as overflowing currents likely formed a freshwater surface layer, reducing ventilation of bottom waters. The formation of the freshwater surface layer and subsequent restricted mixing could have led to pronounced stratification in the water column, with isotopically lighter freshwater dominating the surface waters, which is evidenced by more depleted $\delta^{18}\text{O}$ planktic foraminifera values (between 15 m and the top of the section) (Fig. 6). The subsequent stratification in the water column would have exacerbated the buildup of oxygen-depleted conditions and the isotopically depleted carbon pool

at the bottom. This would also favor sulfate reduction by microbial processes which produce further isotopically light carbon and reduce $\delta^{13}\text{C}$ values in an euxinic benthic environment. Consequently, stratification and reduced oxygenation must have enhanced the preservation of organic matter in bottom sediments.

The decrease in $\delta^{18}\text{O}$ of benthic foraminifera at ca. 22 m is possibly related to the slight warming recorded in the North Sea (Śliwińska et al., 2019) in paleomagnetic Subchron C13n above the EOIS (Fig. 6). The increase in $\delta^{18}\text{O}$ planktic foraminifera after ca. 25 m up to the ca. 40–41 m is likely related to further cooling during the EOGM. A sharp declining trend could be noticed for benthic foraminifera $\delta^{13}\text{C}$ during the onset of this interval (at ca. 25 m), suggesting a relatively less organic carbon burial. This was due to a decrease in primary productivity at the surface represented by lowering $\delta^{13}\text{C}$ of planktic foraminifera and lowered terrestrial input.

The relative sea level in the Paratethys starts to lower after the ca. 40–41 m level (Fig. 3), which is followed by another freshwater input likely due to enhanced precipitation at the level of ca. 45 m. This is evidenced by the depleted $\delta^{18}\text{O}$ planktic foraminifera values and an increase in terrestrial palynomorphs (Figs. 3, 6). Once again this was followed by an increase in organic carbon burial represented by a peak in benthic $\delta^{13}\text{C}$ values at ca. 47 m.

During the Oi-1a cooling (between section levels ca. 45 and 75 m), a long-term declining trend in benthic $\delta^{13}\text{C}$ is distinctive and suggests a decrease in organic carbon burial in the Karaburun area (Fig. 6). The decreasing relative sea level and related increase in bottom current velocities and wave

action combined with a decrease in freshwater input should have likely decreased the organic carbon burial suggested by decreasing benthic $\delta^{13}\text{C}$ at ca. 52–53 m. Another freshwater ingression as surface runoff could be seen at the level of ca. 56 m represented by a sharp decrease in planktic $\delta^{18}\text{O}$ and $\delta^{13}\text{C}$. It appears that the global Oi-1a cooling signal dominates the upper part of the section between levels ca. 60 and 75 m. At ca. 63 m a decrease in planktic $\delta^{18}\text{O}$ and $\delta^{13}\text{C}$ values corresponds to surface freshwater input accompanied by increased organic carbon burial (peak in benthic $\delta^{13}\text{C}$ values). A sharp decline in both benthic and planktic $\delta^{18}\text{O}$ and $\delta^{13}\text{C}$ values suggests a significant freshwater influx at the level of ca. 65 m. The uppermost peak in benthic $\delta^{13}\text{C}$ values at ca. 70 m represents an enhanced organic carbon burial in the Karaburun area due to more favorable conditions for organic carbon sequestration provided by a relative sea-level rise (e.g., lower bottom current velocities and lower wave action).

The divergent trend between benthic and planktic $\delta^{13}\text{C}$ values indicates a highly stratified Paratethys Sea from time to time and different surface and bottom carbon cycling processes after a change from anti-estuarine to estuarine circulation during the EOT. These changes reflect both regional hydrological and basin reconfiguration (restriction) controls and global climatic and eustatic shifts within the EOT. The global cooling during the EOT and Oi-1 must have amplified the stratification, reduced ventilation, and triggered local environmental shifts in the semi-enclosed Paratethys Basin. These environmental shifts provided favorable conditions for the deposition of organic-rich fine-grained sediments with high total organic carbon (TOC) values.

Overall, this contrasting pattern between the isotopic values of benthic and planktic foraminifera highlights the complex interplay of global climate trends (Antarctic glaciation and global cooling) and regional factors (basin isolation and hydrological changes) during the EOT. Our findings align with the proposed isolation of the Paratethys, driven by the prolonged African–Arabian–Eurasian collision coupled with eustatic sea-level decline at the EOB and the cooling during the EOT. In turn this led to the development of a distinct Paratethyan domain marked by mesophilic, humid climatic conditions and intensified runoff (Popov et al., 2002). Moreover, the reconstructed relative sea-level evolution closely corresponds to other reconstructions of relative sea-level changes from the late Eocene to early Oligocene period (e.g., from the Neo-Tethys, Brinkhuis, 1994; North Sea, Jarvse et al., 2015), further reinforcing the presence of a global climatic signal as well.

6.5 Boreal water in the Paratethys during the early Oligocene and its paleoceanographic significance

The prominent negative shift in $\delta^{18}\text{O}$ of benthic foraminifera likely representing the boreal water ingression recorded in the Karaburun composite section shortly after the EOB

(ca. 33.7 Ma) appears to be widespread across the entire Paratethys Basin (Fig. 7; Soták, 2010; Ozsvárt et al., 2016; Gavrilov et al., 2017; van der Boon et al., 2019). In the Eastern Paratethys, this shift appears to have occurred abruptly. A similar negative shift in $\delta^{18}\text{O}$ of bulk carbonates is also recorded further west in the western Alpine foreland basin (Chalufy section, Soutter et al., 2022), which connected the Western Paratethys to the Mediterranean Tethys Ocean (Figs. 7, 8). Hence, boreal water ingression into the Paratethys, beginning in the Eastern Paratethys and progressively reaching the central and western regions, is clearly represented by this negative shift across the entire Paratethys Basin just after the EOB. This process was likely linked to the restriction or closure of the Arctic–Atlantic gateway and the onset of anti-estuarine circulation between the Atlantic and the Nordic Seas during the EOT. Proxy records indicate that the Eocene Arctic Ocean was significantly fresher than today, with salinities ranging from 20 to 25 psu and occasional drops below 10 psu (Brinkhuis et al., 2006; Kim et al., 2014; Waddell and Moore, 2008). The Arctic freshwater outflow into the North Atlantic may have inhibited deep-water formation during the Eocene (Baatsen et al., 2020; Hutchinson et al., 2018). Sea-level and paleo-shoreline reconstructions in the Nordic Seas support the hypothesis that the Arctic became isolated during the latest Eocene to early Oligocene due to the closure of the Arctic–Atlantic gateway (Hegewald and Jokat, 2013; O'Regan et al., 2011; Hutchinson et al., 2019). Recent evidence suggests that the deepening of the Greenland–Scotland Ridge (GSR) around the EOT (just before the EOIS, ca. 33.7 Ma) facilitated increased exchange between the Atlantic and the Nordic Seas, enabling the formation of anti-estuarine circulation and the salinization of North Atlantic surface waters (Abelson and Erez, 2017; Stärz et al., 2017). Consequently, the gradual restriction of Arctic–Atlantic connectivity, followed by the onset of anti-estuarine circulation driven by the deepening of the GSR, may have played a critical role in developing a robust Atlantic Meridional Overturning Circulation (AMOC; e.g., Coxall et al., 2018; Hutchinson et al., 2019). Together, the Atlantic–Arctic closure and onset of anti-estuarine circulation events could have triggered or intensified the AMOC (e.g., Abelson and Erez, 2017; Coxall et al., 2018; Hutchinson et al., 2019). The onset of Nordic anti-estuarine circulation around the EOT might have likely influenced salinity gradients and circulation in connected basins like the North Sea and Paratethys, contributing to the freshening of the latter (Fig. 8). Our data indicate the onset of anti-estuarine circulation in the Paratethys around 33.7 Ma, coinciding with the development of similar circulation patterns between the Nordic Seas and the North Atlantic (Abelson and Erez, 2017). We propose a hypothetical pathway for this circulation: warm surface water entering from the North Sea would have flowed into the eastern Nordic Seas, joining the warm surface waters from the North Atlantic. After losing heat, this water likely sank in the northern Nordic basin; flowed southward as deep wa-

ter; and eventually reached the North Atlantic, the North Sea, the Paratethys, and the Mediterranean Tethys, forming an interhemispheric northern-sourced circulation cell (Fig. 8a).

The onset of anti-estuarine circulation in the Paratethys was likely related to the deepening of the Greenland–Scotland Ridge (GSR), similar to the development of anti-estuarine circulation in the Nordic Seas. During most of the Paleogene, the GSR was shallower, restricting deep-water exchange between the North Atlantic and the Nordic Seas. A key feature of the modern AMOC is the formation of North Atlantic Deep Water, which flows over the GSR from the Nordic Seas. The initiation of Nordic anti-estuarine circulation events around the EOT likely enhanced deep-water formation, strengthening the Atlantic Meridional Overturning Circulation (AMOC) and establishing an interhemispheric northern-sourced circulation cell (e.g., Abelson and Erez, 2017; Coxall et al., 2018; Hutchinson et al., 2019). This suggests that by ~ 33.7 Ma, the Paratethys, with its anti-estuarine circulation, was integrated into this larger circulation system, contributing to global ocean circulation. Shortly after, subsequent geographic restrictions and hydrological changes during the EOT changed this anti-estuarine circulation to an estuarine circulation (Fig. 8b). The closure of the Mediterranean Seaway – along with the narrowing of other seaways likely caused by the major sea-level fall during the EOIS and EOGM – and increased freshwater influxes from the continent diluted the surface Tethyan waters, disrupted the anti-estuarine circulation pattern, and led to brackish surface salinities in the Paratethys (e.g., Schulz et al., 2005; Soták, 2010).

Further evidence supporting boreal water ingression and circulation through the Nordic Seas, North Sea, and Paratethys comes from the distribution of *Svalbardella cooksoniae* in the Greenland, Norwegian, and North Seas, as well as in the Eastern Paratethys during the Oi-1a cooling event (Śliwińska and Heilmann-Clausen, 2011). This suggests a possible migration pathway for *Svalbardella* spp. The presence of *Svalbardella* in the Massicore and Monte Cagnero sections of central Italy (Brinkhuis and Biffi, 1993; Van Mourik and Brinkhuis, 2005) aligns with our interpretation of boreal water circulation extending to the Mediterranean Tethys through the Paratethys (Fig. 8). Sinking cold boreal freshwater likely propagated through interconnected Nordic marine basins, reaching the Paratethys and eventually the Mediterranean Tethys (Fig. 8). The invasion of the Mediterranean Tethys by higher-latitude taxa around the EOB (Brinkhuis and Biffi, 1993) further supports this circulation pathway. The incursion of boreal bottom waters into the Mediterranean Tethys during the EOT is corroborated by a marked transient increase in deep-water ostracod *Krithe* and a decline in deep-water ostracod diversity in the Massignano composite section (Slotnick and Schellenberg, 2013). The *Krithe* pulse and the subtle change in the deep-water ostracod fauna reflect intensified thermohaline flow of cooler deep waters, likely linked to boreal fresh-

water circulation through the Paratethys (e.g., Dall’Antonia et al., 2003; Slotnick and Schellenberg, 2013). Variations in seafloor ventilation and productivity due to changes in paleoceanographic conditions of the Tethys during the late Eocene–early Oligocene described in previous studies (Jovane et al., 2007, and references therein) are also likely related to the circulation of the boreal water.

The influence of boreal waters on the Mediterranean Tethys might also explain the absence of well-defined positive $\delta^{18}\text{O}$ and $\delta^{13}\text{C}$ shifts typically characterizing the EOT in Italian sections, including the GSSP for the EOB (e.g., Houben et al., 2012). Instead, these sections display distinct negative shifts in $\delta^{18}\text{O}$ and $\delta^{13}\text{C}$ bulk carbonate values around the EOB (e.g., Jovane et al., 2007; Brown et al., 2009; Jaramillo-Vogel et al., 2013), resembling the Paratethys records and likely reflecting deep boreal freshwater incursion through the Paratethys.

7 Conclusions

This study provides a comprehensive examination of the EOT and early Oligocene cooling in the Eastern Paratethys, with a focus on the Karaburun composite section. By integrating high-resolution biostratigraphy, geochemistry, sequence stratigraphy, and precise geochronology, we constructed a robust chronostratigraphic framework spanning the latest Eocene to early Oligocene. Our findings reveal that the isotopic shifts in $\delta^{18}\text{O}$ and $\delta^{13}\text{C}$ at the Karaburun site align closely with global records, underscoring the influence of global climatic drivers during this critical transition. However, significant regional deviations, such as depleted $\delta^{18}\text{O}$ values and pronounced stratification, highlight the impact of regional hydrological changes and basin restriction of the Paratethys. These results emphasize the dual influence of global icehouse dynamics and regional hydrological processes on the Paratethys during the EOT. The identification of key cooling events, such as the *Glaphyrocysta semitecta* influx for the EOB and the *Svalbardella* event and its alignment with the Oi-1a glaciation, further enhances the utility of the Karaburun section for refining regional and global stratigraphic correlations. Additionally, the observed sequence stratigraphic patterns illustrate the interplay between eustatic sea-level changes and regional depositional dynamics during this interval. The abrupt depleted values in $\delta^{18}\text{O}$ values in benthic foraminifera just after the EOB (ca. 33.7 Ma) in the Paratethys Basin are attributed to boreal water ingression, driven by the closure of the Arctic–Atlantic gateway and the onset of anti-estuarine circulation between the Nordic Seas and Atlantic during the EOT. This event, which funneled low-salinity boreal water through the Nordic and North Seas into the Paratethys, aligns with the distribution of boreal taxa like *Svalbardella cooksoniae* and extends as far as the Mediterranean Tethys, explaining isotopic anomalies in these regions. We have to note that the large-

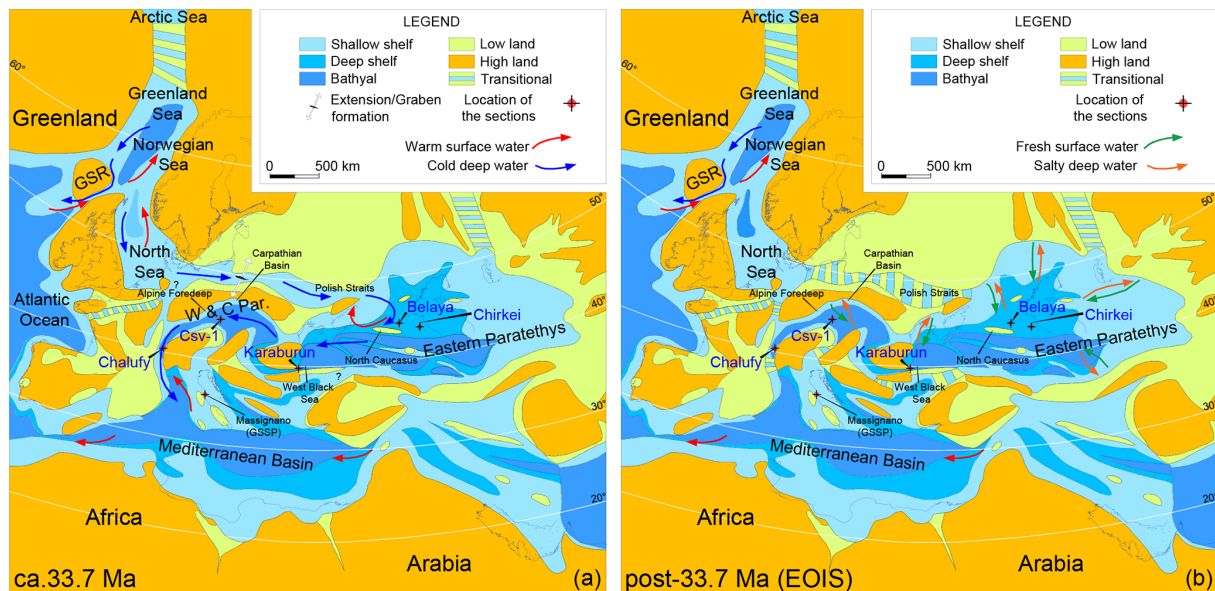


Figure 8. Paleogeographic maps at 33.7 and post-33.7 Ma during the EOIS (the Earliest Oligocene Oxygen Isotope Step) (modified from Sachsenhofer et al., 2018). **(a)** Boreal water anti-estuarine circulation at ca. 33.7 Ma through the Paratethys, extending into the Mediterranean Tethys. GSR: Greenland–Scotland Ridge. **(b)** Estuarine circulation in the Paratethys during the EOIS due to the geographic restrictions (closure of the Mediterranean and other seaways due to the major sea-level fall) and hydrological changes (increased freshwater influx from land).

scale oceanic circulation scenario proposed here requires the movement of deep waters through narrow and shallow seaways surrounding the Paratethys, such as the Polish straits, the Alpine Seaway, and smaller Neo-Tethys–Paratethys gateways. However, the timing of their closure and their paleobathymetry during the early Oligocene remain uncertain, as existing paleogeographic maps for this period are inconsistent (e.g., Barrier et al., 2018; Palcu and Krijgsman, 2023; Straume et al., 2024). Therefore, high-resolution paleogeographic reconstructions, integrated with ocean circulation modeling (e.g., Vahlenkamp et al., 2018), are essential for testing and validating this hypothesis. Overall, the Karaburun section emerges as a critical archive for studying the EOT in epicontinental seas. Our findings contribute to a deeper understanding of how global climatic transitions manifest in marginal marine settings and highlight the potential for further high-resolution studies to refine our knowledge of early icehouse climate evolution in the Paratethys region and beyond.

Data availability. All relevant data are included in the paper and Supplement.

Supplement. The supplement related to this article is available online at <https://doi.org/10.5194/cp-21-1405-2025-supplement>.

Author contributions. MYK designed the study. MYK and SGA conducted fieldwork. TV prepared samples for geochemical analyses. DN performed geochemical analyses. AL conducted geochronological analysis. HB performed the marine palynological analyses. CF analyzed the calcareous nannofossils. MYK wrote the paper with input from all authors. All authors analyzed and discussed the data.

Competing interests. The contact author has declared that none of the authors has any competing interests.

Disclaimer. Publisher's note: Copernicus Publications remains neutral with regard to jurisdictional claims made in the text, published maps, institutional affiliations, or any other geographical representation in this paper. While Copernicus Publications makes every effort to include appropriate place names, the final responsibility lies with the authors.

Acknowledgements. This study is funded by a TÜBİTAK-2236 fellowship and Horizon 2020 Marie Skłodowska-Curie COFUND action (project no. 121C058). We thank Pierre Deschamps and Abel Guihou from the CEREGE Envitop analytical facility for their analytical and administrative support. Envitop has received funding from the Excellence Initiative of Aix Marseille University A*MIDEX – DATCARB project, a French “Investissement d’avenir” program.

Financial support. This research has been supported by a TÜBİTAK-2236 fellowship and the EU Horizon 2020 Marie Skłodowska-Curie COFUND action (grant no. 121C058).

Review statement. This paper was edited by Zhongshi Zhang and reviewed by Noel Vandenbergh and one anonymous referee.

References

- Abels, H. A., Dupont-Nivet, G., Xiao, G., Bosboom, R., and Krijgsman, W.: Step-wise change of Asian interior climate preceding the Eocene–Oligocene Transition (EOT), *Palaeogeogr. Palaeoclimatol.*, 299, 399–412, <https://doi.org/10.1016/j.palaeo.2010.11.028>, 2011.
- Abelson, M. and Erez, J.: The onset of modern-like Atlantic meridional overturning circulation at the Eocene–Oligocene transition: Evidence, causes, and possible implications for global cooling, *Geochim. Geophys. Res.*, 18, 2177–2199, <https://doi.org/10.1002/2017GC006826>, 2017.
- Agnini, C., Fornaciari, E., Raffi, I., Catanzariti, R., Palike, H., Backman, J., and Rio, D.: Biozonation and biochronology of Paleogene calcareous nannofossils from low and middle latitudes, *Newsl. Stratigr.*, 47, 131–181, <https://doi.org/10.1127/0078-0421/2014/0042>, 2014.
- Aubry, M. P.: Late Paleogene Calcareous Nannoplankton Evolution: A Tale of Climatic Deterioration, in: *Eocene–Oligocene Climatic and biotic evolution*, edited by: Prothero D. R. and Berggren W. A., Princeton University Press, Princeton, USA, 272–309, <http://www.jstor.org/stable/j.ct7zvp65.18>, 1992.
- Auer, G., Piller, W. E., and Harzhauser, M.: High-resolution calcareous nannoplankton palaeoecology as a proxy for small-scale environmental changes in the Early Miocene, *Mar. Micropaleontol.*, 111, 53–65, <https://doi.org/10.1016/j.marmicro.2014.06.005>, 2014.
- Baatsen, M., von der Heydt, A. S., Huber, M., Kliphuis, M. A., Bijl, P. K., Sluijs, A., and Dijkstra, H. A.: The middle to late Eocene greenhouse climate modelled using the CESM 1.0.5, *Clim. Past*, 16, 2573–2597, <https://doi.org/10.5194/cp-16-2573-2020>, 2020.
- Backman, J.: Quantitative Calcareous Nannofossil Biochronology of Middle Eocene through Early Oligocene Sediment from DSDP Sites 522 and 523, *Abh. Geol. Bundesanst.*, 39, 21–31, 1987.
- Barrier, E., Vrielynck, B., Brouillet, J. F., and Brunet, M. F.: Paleotectonic Reconstruction of the Central Tethyan Realm. Tectono-Sedimentary-Palinspastic maps from Late Permian to Pliocene, Paris, Atlas of 20 maps (scale: 1 / 15 000 000), <http://www.ccg-m.org> (last access: 12 November 2024), 2018.
- Bartol, M., Pavšič, J., Dobnikar, M., and Bernasconi, S. M.: Unusual *Braarudosphaera bigelowii* and *Micrantholithus vesper* enrichment in the Early Miocene sediments from the Slovenian Corridor, a seaway linking the Central Paratethys and the Mediterranean, *Palaeogeogr. Palaeoclimatol.*, 267, 77–88, <https://doi.org/10.1016/j.palaeo.2008.06.005>, 2008.
- Bati, Z.: Dinoflagellate cyst biostratigraphy of the upper Eocene and lower Oligocene of the Kirmizitepe Section, Azerbaijan, South Caspian Basin, *Rev. Palaeobot. Palynol.*, 217, 9–38, <https://doi.org/10.1016/j.revpalbo.2015.03.002>, 2015.
- Bijl, P. K., Brinkhuis, H., Egger, L. M., Eldrett, J. S., Frieling, J., Grothe, A., Houben, A. J. P., Pross, J., Śliwińska, K. K., and Sluijs, A.: Comment on “*Wetzelioella* and its allies—the “hole” story: a taxonomic revision of the Paleogene dinoflagellate sub-family Wetzelioelloideae” by Williams et al. (2015), *Palynology*, 41, 423–429, <https://doi.org/10.1080/01916122.2016.1235056>, 2017.
- Brinkhuis, H.: Late Eocene to early Oligocene dinoflagellate cysts from the Priabonian type-area (Northeast Italy): biostratigraphy and paleoenvironmental interpretation, *Palaeogeogr. Palaeoclimatol.*, 107, 121–163, [https://doi.org/10.1016/0031-0182\(94\)90168-6](https://doi.org/10.1016/0031-0182(94)90168-6), 1994.
- Brinkhuis, H. and Biffi, U.: Dinoflagellate cyst stratigraphy of the Eocene/Oligocene transition in central Italy, *Mar. Micropaleontol.*, 22, 131–183, [https://doi.org/10.1016/0377-8398\(93\)90007-K](https://doi.org/10.1016/0377-8398(93)90007-K), 1993.
- Brinkhuis, H. and Visscher, H.: The upper boundary of the Eocene Series: a reappraisal based on dinoflagellate cyst biostratigraphy and sequence stratigraphy, in: *Geochronology, Time Scales and Global Stratigraphic Correlation*, edited by: Berggren, W. A., Kent, D. V., Aubry, M.-P., and Hardenbol, J., SEPM, Special Publication, SEPM Society for Sedimentary Geology, 54, 295–304, <https://doi.org/10.2110/pec.95.04.0295>, 1995.
- Brinkhuis, H., Schouten, S., Collinson, M. E., Sluijs, A., Damsté, J. S. S., Dickens, G. R., Huber, M., Cronin, T. M., Onodera, J., Takahashi, K., Bujak, J. P., Stein, R., van der Burgh, J., Eldrett, J. S., Harding, I. C., Lotter, A. F., Sangiorgi, F., van Konijnenburg-van Cittert, H., de Leeuw, J. W., Matthiessen, J., Backman, J., Moran, K., and Expedition 302 Scientists: Episodic fresh surface waters in the Eocene Arctic Ocean, *Nature*, 441, 606–609, <https://doi.org/10.1038/nature04692>, 2006.
- Bordiga, M., Henderiks, J., Tori, F., Monechi, S., Fenner, R., Legarda-Lisarrri, A., and Thomas, E.: Microfossil evidence for trophic changes during the Eocene–Oligocene transition in the South Atlantic (ODP Site 1263, Walvis Ridge), *Clim. Past*, 11, 1249–1270, <https://doi.org/10.5194/cp-11-1249-2015>, 2015.
- Boulila, S., Dupont-Nivet, G., Galbrun, B., Bauer, H., and Châteauneuf, J.-J.: Age and driving mechanisms of the Eocene–Oligocene transition from astronomical tuning of a lacustrine record (Rennes Basin, France), *Clim. Past*, 17, 2343–2360, <https://doi.org/10.5194/cp-17-2343-2021>, 2021.
- Bown, P. R.: Palaeogene calcareous nannofossils from the Kilwa and Lindi areas of coastal Tanzania (Tanzania Drilling Project Sites 1 to 10, 2003–4), *J. Nannoplankton Res.*, 27, 21–95, <https://doi.org/10.58998/jnr2031>, 2005.
- Bown, P. R. and Pearson, P.: Calcareous plankton evolution and the Paleocene/Eocene thermal maximum event: New evidence from Tanzania, *Mar. Micropaleontol.*, 71, 60–70, <https://doi.org/10.1016/j.marmicro.2009.01.005>, 2009.
- Bown, P. R. and Young, J. R.: Techniques, in: *Calcareous nannofossil biostratigraphy*, edited by: Bown, P. R., Chapman & Hall, Cambridge, UK, 16–28, ISBN 0-412-78970-1, 1998.
- Brown, R. E., Koeberl, C., Montanari, A., and Bice, D. M.: Evidence for a change in Milankovitch forcing caused by extraterrestrial events at Massignano, Italy, Eocene–Oligocene boundary GSSP, in: *The Late Eocene Earth-Hothouse, Icehouse, and Impacts*, edited by: Koeberl, C. and Montanari, A., Geol. Soc. Am. Bull., 452, 1–19, [https://doi.org/10.1130/2009.2452\(08\)](https://doi.org/10.1130/2009.2452(08)), 2009.

- Catanzariti, R., Rio, D., and Martelli, L.: Late Eocene to Oligocene calcareous nannofossil Biostratigraphy in Northern Apennines: the Ranzano sandstone, *Mem. Sci. Geol.*, 49, 207–253, 1997.
- Cattò, S., Cavazza, W., Zattin, M., and Okay, A. I.: No significant Alpine tectonic overprint on the Cimmerian Strandja Massif (SE Bulgaria and NW Turkey), *Int. Geol. Rev.*, 60, 513–529, <https://doi.org/10.1080/00206814.2017.1350604>, 2018.
- Catuneanu, O. (Ed.): Principles of sequence stratigraphy, Elsevier, Amsterdam, the Netherlands, 375 pp., ISBN 9780444515681, 2006.
- Caves, J. K., Jost, A. B., Lau, K. V., and Maher, K.: Cenozoic carbon cycle imbalances and a variable weathering feedback, *Earth Planet. Sci. Lett.*, 450, 152–163, <https://doi.org/10.1016/j.epsl.2016.06.035>, 2016.
- Chekar, M., Slimani, H., Jbari, H., Guédé, K. E., Mahboub, I., Asebriy, L., and Aassoumi, H.: Eocene to Oligocene dinoflagellate cysts from the Tattofte section, western External Rif, northwestern Morocco: Biostratigraphy, paleoenvironments and paleoclimate, *Palaeogeogr. Palaeoclimatol.*, 507, 97–114, <https://doi.org/10.1016/j.palaeo.2018.07.004>, 2018.
- Coxall, H. K. and Pearson, P. N.: The Eocene–Oligocene transition, in: Deep Time Perspectives on Climate Change: Marrying the Signal From Computer Models and Biological Proxies, edited by: Williams, M., Haywood, A. M., Gregory, F. J., and Schmidt, D. N., The Micropalaeontological Society, Special Publications, Geological Society of London, 2, 351–387, <https://doi.org/10.1144/TMS002.16>, 2007.
- Coxall, H. K. and Wilson, P. A.: Early Oligocene glaciation and productivity in the eastern equatorial Pacific: Insights into global carbon cycling, *Paleoceanography*, 26, 1–18, <https://doi.org/10.1029/2010PA002021>, 2011.
- Coxall, H. K., Wilson, P. A., Pälike, H., Lear, C. H., and Backman, J.: Rapid stepwise onset of Antarctic glaciation and deeper calcite compensation in the Pacific Ocean, *Nature*, 433, 53–57, <https://doi.org/10.1038/nature03135>, 2005.
- Coxall, H. K., Huck, C. E., Huber, M., Lear, C. H., Legarda-Lisarrri, A., O'regan, M., Sliwinski, K. K., van de Flierdt, T., de Boer, A. M., Zachos, J. C., and Backman, J.: Export of nutrient rich Northern Component Water preceded early Oligocene Antarctic glaciation, *Nat. Geosci.*, 11, 190–196, <https://doi.org/10.1038/s41561-018-0069-9>, 2018.
- Cramwinckel, M. J., Coxall, H. K., Śliwińska, K. K., Polling, M., Harper, D. T., Bijl, P. K., Brinkhuis, H., Eldrett, J. S., Houben, A. J. P., Peterse, F., Schouten, S., Reichert, G.-J., Zachos, J. C., and Sluijs, A.: A warm, stratified, and restricted Labrador Sea across the Middle Eocene and its climatic optimum, *Paleoceanogr. Paleoclimatol.*, 35, 1–27, <https://doi.org/10.1029/2020PA003932>, 2020.
- Cunha, A. S. and Shimabukuro, S.: *Braarudosphaera* blooms and anomalous enrichments of *Nannoconus*: Evidence from the Turonian South Atlantic, Santos Basin, Brazil, *J. Nanoplankton Res.*, 19, 51–55, <https://doi.org/10.58998/jnr2217>, 1997.
- Dall'Antonia, B., Bossio, A., and Guernet, C.: The Eocene/Oligocene boundary and the psychrospheric event in the Tethys as recorded by deep-sea ostracods from the Massignano Global Boundary Stratotype Section and Point, Central Italy, *Mar. Micropaleontol.*, 48, 91–106, [https://doi.org/10.1016/S0377-8398\(02\)00163-9](https://doi.org/10.1016/S0377-8398(02)00163-9), 2003.
- Dansgaard, W.: Stable isotopes in precipitation, *Tellus*, 16, 436–468, <https://doi.org/10.3402/tellusa.v16i4.8993>, 1964.
- De Kaenel, E. and Villa, G.: Oligocene–Miocene calcareous nannofossil biostratigraphy and paleoecology from the Iberia Abyssal Plain, in: Proceedings–Ocean Drilling Program Scientific Results vol. 149, edited by: Whitmarsh, R. B., Sawyer, D. S., Klaus, A., and Masson, D. G., College Station, TX, 79–146, <https://doi.org/10.2973/odp.proc.sr.149.208.1996>, 1996.
- De Lira Mota, M. A., Dunkley Jones, T., Sulaiman, N., Edgar, K. M., Yamaguchi, T., Leng, M. J., Adloff, M., Greene, S. E., Norris, R., Warren, B., Duffy, G., Farrant, J., Murayama, M., Hall, J., and Bendle, J.: Multi-proxy evidence for sea level fall at the onset of the Eocene–Oligocene transition, *Nat. Commun.*, 14, 4748, <https://doi.org/10.1038/s41467-023-39806-6>, 2023.
- Dickson, A. J., Bagard, M. L., Katchinoff, J. A., Davies, M., Poulton, S. W., and Cohen, A. S.: Isotopic constraints on ocean redox at the end of the Eocene, *Earth Planet. Sci. Lett.*, 562, 116814, <https://doi.org/10.1016/j.epsl.2021.116814>, 2021.
- Diester-Haass, L. and Zahn, R.: Eocene–Oligocene transition in the Southern Ocean: History of water mass circulation and biological productivity, *Geology*, 24, 163–166, [https://doi.org/10.1130/0091-7613\(1996\)024<0163:EOTITS>2.3.CO;2](https://doi.org/10.1130/0091-7613(1996)024<0163:EOTITS>2.3.CO;2), 1996.
- Dohmann, L.: Die unteroligozänen Fische im Molassebecken, Dissertation, Ludwig-Maximilian-Universität, Munich, Germany, 365 pp., 1991.
- Dunkley Jones, T., Bown, P. R., Pearson, P. N., Wade, B. S., Coxall, H. K., and Lear, C. H.: Major shifts in calcareous phytoplankton assemblages through the Eocene–Oligocene transition of Tanzania and their implications for low-latitude primary production, *Paleoceanography*, 23, 1–14, <https://doi.org/10.1029/2008PA001640>, 2008.
- El Beialy, S. Y., Head, M. J., El Atfy, H., and El Khoriby, E. M.: Dinoflagellate cyst evidence for the age and palaeoenvironments of the Upper Eocene–Oligocene Dabaa Formation, Qattara Depression, north Western Desert, Egypt, *Palynology*, 43, 268–291, <https://doi.org/10.1080/01916122.2018.1434696>, 2019.
- Eldrett, J. S., Harding, I. C., Firth, J. V., and Roberts, A. P.: Magnetostratigraphic calibration of Eocene–Oligocene dinoflagellate cyst biostratigraphy from the Norwegian–Greenland Sea, *Mar. Geol.*, 204, 91–127, [https://doi.org/10.1016/S0025-3227\(03\)00357-8](https://doi.org/10.1016/S0025-3227(03)00357-8), 2004.
- Eldrett, J. S., Greenwood, D. R., Harding, I. C., and Huber, M.: Increased seasonality through the Eocene to Oligocene transition in northern high latitudes, *Nature*, 459, 969–973, <https://doi.org/10.1038/nature08069>, 2009.
- Ferreira, E. P., Alves, C. F., Sanjinés, A. E. S., and Alves, M. C.: Ascidian spicules of Quaternary sediments from the lower slope of the Campos Basin (Brazil), *Quatern. Int.*, 508, 116–124, <https://doi.org/10.1016/j.quaint.2018.11.008>, 2019.
- Fioroni, C., Villa, G., Persico, D., and Jovane, L.: Middle Eocene–Lower Oligocene calcareous nannofossil biostratigraphy and paleoceanographic implications from Site 711 (equatorial Indian Ocean), *Mar. Micropaleontol.*, 118, 50–62, <https://doi.org/10.1016/j.marmicro.2015.06.001>, 2015.
- Frieling, J. and Sluijs, A.: Towards quantitative environmental reconstructions from ancient non-analogue microfossil assemblages: Ecological preferences of Paleocene–Eocene dinoflagellates, *Earth-Sci. Rev.*, 185, 956–973, <https://doi.org/10.1016/j.earscirev.2018.08.014>, 2018.

- Gat, J. R.: Oxygen and hydrogen isotopes in the hydrologic cycle, *Annu. Rev. Earth Planet. Sc.*, 24, 225–262, <https://doi.org/10.1146/annurev.earth.24.1.225>, 1996.
- Gavrilov, Y. O., Shchepetova, E. V., Shcherbinina, E. A., Golovanova, O. V., Nedumov, R. I., and Pokrovsky, B. G.: Sedimentary environments and geochemistry of Upper Eocene and Lower Oligocene rocks in the north-eastern Caucasus, *Lithol. Miner. Resour.*, 52, 447–466, <https://doi.org/10.1134/S0024490217060037>, 2017.
- Gradstein, F. M., Ogg, J. G., Schmitz, M. D., and Ogg, G. E. (Eds.): *The geologic time scale*, Boston, USA, 1144 pp., ISBN 978-0-444-59425-9, 2012.
- Guerreiro, C., Cachão, M., and Drago, T.: Calcareous nannoplankton as a tracer of the marine influence on the NW coast of Portugal over the last 14000 years, *J. Nannoplankton Res.*, 27, 159–172, <https://doi.org/10.58998/jnr2107>, 2005.
- Haidar, A. T. and Thierstein, H. R.: Coccolithophore dynamics off Bermuda (N. Atlantic), *Deep-Sea Res. Pt. II*, 48, 1925–1956, [https://doi.org/10.1016/S0967-0645\(00\)00169-7](https://doi.org/10.1016/S0967-0645(00)00169-7), 2001.
- Haq, B. U.: Biogeographic history of Miocene calcareous nannoplankton and paleoceanography of the Atlantic Ocean, *Micropaleontology*, 26, 414–443, <https://doi.org/10.2307/1485353>, 1980.
- Hegewald, A. and Jokat, W.: Relative sea level variations in the Chukchi region-Arctic Ocean-since the late Eocene, *Geophys. Res. Lett.*, 40, 803–807, <https://doi.org/10.1002/grl.50182>, 2013.
- Hou, M., Zhuang, G., Ellwood, B. B., Liu, X. L., and Wu, M.: Enhanced precipitation in the Gulf of Mexico during the Eocene–Oligocene transition driven by interhemispherical temperature asymmetry, *Geol. Soc. Am. Bull.*, 134, 2335–2344, <https://doi.org/10.1130/B36103.1>, 2022.
- Houben, A. J., van Mourik, C. A., Montanari, A., Coccioni, R., and Brinkhuis, H.: The Eocene–Oligocene transition: Changes in sea level, temperature or both?, *Palaeogeogr. Palaeoclimatol.*, 335, 75–83, <https://doi.org/10.1016/j.palaeo.2011.04.008>, 2012.
- Hutchinson, D. K., de Boer, A. M., Coxall, H. K., Caballero, R., Nilsson, J., and Baatsen, M.: Climate sensitivity and meridional overturning circulation in the late Eocene using GFDL CM2.1, *Clim. Past*, 14, 789–810, <https://doi.org/10.5194/cp-14-789-2018>, 2018.
- Hutchinson, D. K., Coxall, H. K., O'Regan, M., Nilsson, J., Caballero, R., and de Boer, A. M.: Arctic closure as a trigger for Atlantic overturning at the Eocene–Oligocene Transition, *Nat. Commun.*, 10, 3797, <https://doi.org/10.1038/s41467-019-11828-z>, 2019.
- Hutchinson, D. K., Coxall, H. K., Lunt, D. J., Steinthorsdottir, M., de Boer, A. M., Baatsen, M., von der Heydt, A., Huber, M., Kennedy-Asser, A. T., Kunzmann, L., Ladant, J.-B., Lear, C. H., Moraweck, K., Pearson, P. N., Piga, E., Pound, M. J., Salzmann, U., Scher, H. D., Sijp, W. P., Śliwińska, K. K., Wilson, P. A., and Zhang, Z.: The Eocene–Oligocene transition: a review of marine and terrestrial proxy data, models and model–data comparisons, *Clim. Past*, 17, 269–315, <https://doi.org/10.5194/cp-17-269-2021>, 2021.
- Hyeong, K., Kuroda, J., Seo, I., and Wilson, P. A.: Response of the Pacific inter-tropical convergence zone to global cooling and initiation of Antarctic glaciation across the Eocene Oligocene Transition, *Sci. Rep.*, 6, 30647, <https://doi.org/10.1038/srep30647>, 2016.
- Iakovleva, A. I.: Organic walled dinoflagellate cyst biostratigraphy of the Bartonian/Priabonian GSSP Alano di Piave section, NE Italy, *Rev. Palaeobot. Palynol.*, 332, 105233, <https://doi.org/10.1016/j.revpalbo.2024.105233>, 2025.
- Iakovleva, A. I., Zakrevskaya, E. Y., and Shcherbinina, E. A.: Middle Eocene to earliest Oligocene dinoflagellate cysts from southern Armenia: biostratigraphy and palaeoecology, *Palynology*, 48, 2343902, <https://doi.org/10.1080/01916122.2024.2343902>, 2024.
- Jaramillo-Vogel, D., Strasser, A., Frijia, G., and Spezzaferri, S.: Neritic isotope and sedimentary records of the Eocene–Oligocene greenhouse–icehouse transition: The Calcare di Nago Formation (northern Italy) in a global context, *Palaeogeogr. Palaeoclimatol.*, 369, 361–376, <https://doi.org/10.1016/j.palaeo.2012.11.003>, 2013.
- Jarsve, E. M., Eidvin, T., Nystuen, J. P., Faleide, J. I., Gabrielsen, R. H., and Thyberg, B. I.: The Oligocene succession in the eastern North Sea: basin development and depositional systems, *Geol. Mag.*, 152, 668–693, <https://doi.org/10.1017/S0016756814000570>, 2015.
- Jones, A. P., Dunkley Jones, T., Coxall, H., Pearson, P. N., Nala, D., and Hoggett, M.: Low-latitude calcareous nannofossil response in the Indo-Pacific warm pool across the Eocene–Oligocene transition of Java, Indonesia, *Paleoceanogr. Paleoclimatol.*, 34, 1833–1847, <https://doi.org/10.1029/2019PA003597>, 2019.
- Jovane, L., Florindo, F., Sprovieri, M., and Pälike, H.: Astronomic calibration of the late Eocene/early Oligocene Massignano section (central Italy), *Geochem. Geophys. Geosyst.*, 7, 1–10, <https://doi.org/10.1029/2005GC001195>, 2006.
- Jovane, L., Sprovieri, M., Florindo, F., Acton, G., Coccioni, R., Dall'Antonia, B., and Dinarès-Turell, J.: Eocene–Oligocene paleoceanographic changes in the stratotype section, Massignano, Italy: Clues from rock magnetism and stable isotopes, *J. Geophys. Res.-Sol. Ea.*, 112, B11101, <https://doi.org/10.1029/2007JB004963>, 2007.
- Katz, M. E., Miller, K. G., Wright, J. D., Wade, B. S., Browning, J. V., Cramer, B. S., and Rosenthal, Y.: Stepwise transition from the Eocene greenhouse to the Oligocene icehouse, *Nat. Geosci.*, 1, 329–334, <https://doi.org/10.1038/ngeo179>, 2008.
- Kim, S. L., Eberle, J. J., Bell, D. M., Fox, D. A., and Padilla, A.: Evidence from shark teeth for a brackish Arctic Ocean in the Eocene greenhouse, *Geology*, 42, 695–698, <https://doi.org/10.1130/G35675.1>, 2014.
- Kocsis, L., Ozsvárt, P., Becker, D., Ziegler, R., Scherler, L., and Codrea, V.: Orogeny forced terrestrial climate variation during the late Eocene–early Oligocene in Europe, *Geology*, 42, 727–730, <https://doi.org/10.1130/G35673.1>, 2014.
- Konno, S., Harada, N., Narita, H., and Jordan, R. W.: Living *Braarudosphaera bigelowii* (Gran & Braarud) Deflandre in the Bering Sea, *J. Nannoplankton Res.*, 29, 78–87, <https://doi.org/10.58998/jnr2152>, 2007.
- Langton, S. J., Rabideaux, N. M., Borrelli, C., and Katz, M. E.: Southeastern Atlantic deep-water evolution during the late-middle Eocene to earliest Oligocene (Ocean Drilling program site 1263 and Deep Sea Drilling project site 366), *Geosphere*, 12, 1032–1047, <https://doi.org/10.1130/GES01268.1>, 2016.
- Less, G., Özcan, E., and Okay, A.: Stratigraphy and larger foraminifera of the Middle Eocene to Lower Oligocene shallow-marine units in the northern and eastern parts of the

- Thrace Basin, NW Turkey, *Turk. J. Earth Sci.*, 20, 793–845, <https://doi.org/10.3906/yer-1010-53>, 2011.
- Li, S., Xing, Y., Valdes, P. J., Huang, Y., Su, T., Farnsworth, A., Lunt, D. J., Tang, H., Kennedy, A. T., and Zhou, Z.: Oligocene climate signals and forcings in Eurasia revealed by plant macrofossil and modelling results, *Gondwana Res.*, 61, 115–127, <https://doi.org/10.1016/j.gr.2018.04.015>, 2018.
- Licht, A., Folch, A., Sylvestre, F., Yacoub, A. N., Cogné, N., Abderamane, M., Guihou, A., Kisne, N. M., Fleury, J., Rochette, P., Nké, B. E. B., Zagalo, A. H., Poujol M., and Deschamps, P.: Provenance of aeolian sands from the southeastern Sahara from a detrital zircon perspective, *Quaternary Sci. Rev.*, 328, 108539, <https://doi.org/10.1016/j.quascirev.2024.108539>, 2024.
- Mahboub, I., Slimani, H., Toufiq, A., Chekar, M., Djeya, K. L., Jbari, H., and Chakir, S.: Middle Eocene to early Oligocene dinoflagellate cyst biostratigraphy and paleoenvironmental interpretations of the Ben Attaya section at Taza, eastern External Rif, Morocco, *J. Afr. Earth Sci.*, 149, 154–169, <https://doi.org/10.1016/j.jafrearsci.2018.08.006>, 2019.
- Marchev, P., Raicheva, R., Jicha, B., Guillong, M., Ivanova, R., Bachmann, O., Spikings, R., Okay, A., and Ozsvárt, P.: The large Rupelian Rhodope Massif eruptions as the source of airfall tuffs in SE, S and Central Europe: 40Ar/39Ar and U–Pb age constraints, *Int. J. Earth Sci.*, 113, 1619–1641, <https://doi.org/10.1007/s00531-024-02457-z>, 2024.
- Marino, M. and Flores, J. A.: Middle Eocene to early Oligocene calcareous nannofossil stratigraphy at Leg 177 Site 1090, *Mar. Micropaleontol.*, 45, 383–398, [https://doi.org/10.1016/S0377-8398\(02\)00036-1](https://doi.org/10.1016/S0377-8398(02)00036-1), 2002.
- Marret, F. and De Vernal, A.: Dinoflagellate cysts as proxies of environmental, ocean and climate changes in the Atlantic realm during the quaternary, *Front. Ecol. Environ.*, 12, 1378931, <https://doi.org/10.3389/fevo.2024.1378931>, 2024.
- Martini, E.: Standard Tertiary and Quaternary calcareous nannoplankton zonation, in: *Proceedings second planktonic conference*, Rome, Italy, 1970, 739–785, 1971.
- Miller, K. G., Wright, J. D., and Fairbanks, R. G.: Unlocking the ice house: Oligocene–Miocene oxygen isotopes, eustasy, and margin erosion, *J. Geophys. Res.–Sol. Ea.*, 96, 6829–6848, <https://doi.org/10.1029/90JB02015>, 1991.
- Miller, K. G., Browning, J. V., Aubry, M. P., Wade, B. S., Katz, M. E., Kulpecz, A. A., and Wright, J. D.: Eocene–Oligocene global climate and sea-level changes: St. Stephens Quarry, Alabama, *Geol. Soc. Am. Bull.*, 120, 34–53, <https://doi.org/10.1130/B26105.1>, 2008.
- Miller, K. G., Browning, J. V., Schmelz, W. J., Kopp, R. E., Mountain, G. S., and Wright, J. D.: Cenozoic sea-level and cryospheric evolution from deep-sea geochemical and continental margin records, *Sci. Adv.*, 6, eaaz1346, <https://doi.org/10.1126/sciadv.aaz1346>, 2020.
- Monechi, S., Bucciatti, A., and Gardin, S.: Biotic signals from nannoflora across the iridium anomaly in the upper Eocene of the Massignano section: evidence from statistical analysis, *Mar. Micropaleontol.*, 39, 219–237, [https://doi.org/10.1016/S0377-8398\(00\)00022-0](https://doi.org/10.1016/S0377-8398(00)00022-0), 2000.
- Natal'in, B. and Say, A. G.: Eocene–Oligocene stratigraphy and structural history of the Karaburun area, south-western Black Sea coast, Turkey: transition from extension to compression, *Geol. Mag.*, 152, 1104–1122, <https://doi.org/10.1017/S0016756815000229>, 2015.
- Okay, A. I. and Nikishin, A. M.: Tectonic evolution of the southern margin of Laurasia in the Black Sea region, *Int. Geol. Rev.*, 57, 1051–1076, <https://doi.org/10.1080/00206814.2015.1010609>, 2015.
- Okay, A. I., Özcan, E., Hakyemez, A., Siyako, M., Sunal, G., and Kylander-Clark, A. R.: The Thrace Basin and the Black Sea: the Eocene–Oligocene marine connection, *Geol. Mag.*, 156, 39–61, <https://doi.org/10.1017/S0016756817000772>, 2019.
- Okay, A. I., Simmons, M. D., Özcan, E., Starkie, S., Bidgood, M. D., and Kylander-Clark, A. R.: Eocene–Oligocene succession at Kıyıköy (Midye) on the Black Sea coast in Thrace, *Turk. J. Earth Sci.*, 29, 139–153, <https://doi.org/10.3906/yer-1907-5>, 2020.
- O'Regan, M., Williams, C. J., Frey, K. E., and Jakobsson, M.: A synthesis of the long-term paleoclimatic evolution of the Arctic, *Oceanography*, 24, 66–80, <https://doi.org/10.5670/oceanog.2011.57>, 2011.
- Ozsvárt, P., Kocsis, L., Nyerges, A., Györi, O., and Pálffy, J.: The eocene-oligocene climate transition in the central Paratethys, *Palaeogeogr. Palaeoclimatol.*, 459, 471–487, <https://doi.org/10.1016/j.palaeo.2016.07.034>, 2016.
- Palcu, D. V. and Krijgsman, W.: The dire straits of Paratethys: Gateways to the anoxic giant of Eurasia, in: *Straits and Seaways: Controls, Processes and Implications in Modern and Ancient Systems*, edited by: Rossi, V. M., Longhitano, S. G., Olariu, C., and Chiocci, F. L., Geological Society, London, Special Publications, 523, <https://doi.org/10.1144/SP523-2021-73>, 2023.
- Pälike, H., Norris, R. D., Herrle, J. O., Wilson, P. A., Coxall, H. K., Lear, C. H., Shackleton, N. J., Tripathi, A. K., and Wade, B. S.: The heartbeat of the Oligocene climate system, *Science*, 314, 1894–1898, <https://doi.org/10.1126/science.1133822>, 2006.
- Pearson, P. N., McMillan, I. K., Wade, B. S., Jones, T. D., Coxall, H. K., Bown, P. R., and Lear, C. H.: Extinction and environmental change across the Eocene–Oligocene boundary in Tanzania, *Geology*, 36, 179–182, <https://doi.org/10.1130/G24308A.1>, 2008.
- Pekar, S. and Miller, K. G.: New Jersey Oligocene “Icehouse” sequences (ODP Leg 150X) correlated with global $\delta^{18}\text{O}$ and Exxon eustatic records, *Geology*, 24, 567–570, [https://doi.org/10.1130/0091-7613\(1996\)024<0567:NJOISO>2.3.CO;2](https://doi.org/10.1130/0091-7613(1996)024<0567:NJOISO>2.3.CO;2), 1996.
- Pekar, S. F., Christie-Blick, N., Kominz, M. A., and Miller, K. G.: Calibration between eustatic estimates from backstripping and oxygen isotopic records for the Oligocene, *Geology*, 30, 903–906, [https://doi.org/10.1130/0091-7613\(2002\)030<0903:CBEEFB>2.0.CO;2](https://doi.org/10.1130/0091-7613(2002)030<0903:CBEEFB>2.0.CO;2), 2002.
- Peleo-Alampay, A. M., Mead, G. A., and Wei, W.: Unusual Oligocene *Braarudosphaera*-rich layers of the South Atlantic and their palaeoceanographic implications, *J. Nannoplankton Res.*, 21, 17–26, <https://doi.org/10.58998/jnr2190>, 1999.
- Perch-Nielsen, K.: Cenozoic calcareous nannofossils, in: *Plankton Stratigraphy*, edited by: Bolli, H. M., Saunders, J. B., and Perch-Nielsen, K., Cambridge University Press, Cambridge, UK, 427–554, ISBN-10:0521235766, 1985.
- Pross, J. and Brinkhuis, H.: Organic-walled dinoflagellate cysts as paleoenvironmental indicators in the Paleogene, a synopsis of concepts, *Paläontol. Z.*, 79, 53–59, <https://doi.org/10.1007/BF03021753>, 2005.

- Popov, S. V., Akhmetiev, M. A., Bugrova, E. M., Lopatin, A. V., Amitrov, O. V., Andreyeva-Grigorovich, A. S., Zaporozhets, N. I., Zherikhin, V. V., Krashennnikov, V. A., Nikolaeva, I. A., Sytchevskaya, E. K., and Shcherba, I. G.: Biogeography of the Northern Peri-Tethys from the Late Eocene to the Early Miocene: Part 2. Early Oligocene, *Paleontol. J.*, 36, 185–259, 2002.
- Popov, S. V., Rozanov, A. Y., Rögl, F., Steininger, F. F., Shcherba, I. G., and Kovac, M.: Lithological-paleogeographic maps of Paratethys, CFS Courier Forschungsinstitut Senckenberg, Stuttgart, 250, 46 pp., ISBN 978-3-510-61370-0, 2004.
- Popov, S. V., Antipov, M. P., Zastrozhnov, A. S., Kurina, E. E., and Pinchuk, T. N.: Sea-level fluctuations on the northern shelf of the Eastern Paratethys in the Oligocene-Neogene, *Stratigr. Geol. Correl.*, 18, 200–224, <https://doi.org/10.1134/S0869593810020073>, 2010.
- Raffi, I., Catelli, V., Fioroni, C., Righi, D., Villa, G., and Persico, D.: Calcareous nannofossils from the Paleogene Southern Ocean (IODP Site U1553, Campbell Plateau), *Newsl. Stratigr.*, 57, 475–495, <https://doi.org/10.1127/nos/2024/0854>, 2024.
- Sachsenhofer, R. F., Popov, S. V., Bechtel, A., Coric, S., Francu, J., Gratzner, R., Grunert, P., Kotarba, M., Mayer, J., Pupp, M., Rupprecht B. J., and Vincent, S. J.: Oligocene and Lower Miocene source rocks in the Paratethys: palaeogeographical and stratigraphic controls, Geological Society, London, Special Publications, 464, 267–306, <https://doi.org/10.1144/SP464.1>, 2018.
- Salamy, K. A. and Zachos, J. C.: Latest Eocene–Early Oligocene climate change and Southern Ocean fertility: inferences from sediment accumulation and stable isotope data, *Palaeogeogr. Palaeoclimatol.*, 145, 61–77, [https://doi.org/10.1016/S0031-0182\(98\)00093-5](https://doi.org/10.1016/S0031-0182(98)00093-5), 1999.
- Sancay, R. H. and Batu, Z.: Late Eocene to Early Oligocene palynostratigraphy of the Western Black Sea, Eastern Paratethys, *Turk. J. Earth Sci.*, 29, 115–138, <https://doi.org/10.3906/yer-1905-10>, 2020.
- Scher, H. D., Bohaty, S. M., Zachos, J. C., and Delaney, M. L.: Two-stepping into the icehouse: East Antarctic weathering during progressive ice-sheet expansion at the Eocene–Oligocene transition, *Geology*, 39, 383–386, <https://doi.org/10.1130/G31726.1>, 2011.
- Schulz, H. M., Bechtel, A., and Sachsenhofer, R. F.: The birth of the Paratethys during the Early Oligocene: from Tethys to an ancient Black Sea analogue?, *Global Planet. Change*, 49, 163–176, <https://doi.org/10.1016/j.gloplacha.2005.07.001>, 2005.
- Simmons, M. D., Bidgood, M. D., Connell, P. G., Coric, S., Okay, A. I., Shaw, D., Tulan, E., Mayer, J., and Tari, G. C.: Biostratigraphy and paleoenvironments of the Oligocene succession (İhsaniye Formation) at Karaburun (NW Turkey), *Turk. J. Earth Sci.*, 29, 28–63, <https://doi.org/10.3906/yer-1907-7>, 2020.
- Slimani, H., Mahboub, I., Toufiq, A., Jbari, H., Chakir, S., and Tahiri, A.: Bartonian to Priabonian dinoflagellate cyst biostratigraphy and paleoenvironments of the M'karcha section in the Southern Tethys margin (Rif Chain, Northern Morocco), *Mar. Micropaleontol.*, 153, 101785, <https://doi.org/10.1016/j.marmicro.2019.101785>, 2019.
- Slimani, H. and Chekar, M.: Dinoflagellate-based age control and biostratigraphic correlations of the Eocene and Oligocene (Lutetian–Chattian) sediments in the El Hatt tectonic Unit, western External Rif Chain, Morocco (NW Africa), *Newsl. Stratigr.*, 56, 257–305, <https://doi.org/10.1127/nos/2022/0704>, 2023.
- Śliwińska, K. K.: Early Oligocene dinocysts as a tool for palaeoenvironment reconstruction and stratigraphical framework – a case study from a North Sea well, *J. Micropaleontol.*, 38, 143–176, <https://doi.org/10.5194/jm-38-143-2019>, 2019.
- Śliwińska, K. K. and Heilmann-Clausen, C.: Early Oligocene cooling reflected by the dinoflagellate cyst *Svalbardella cooksoniae*, *Palaeogeogr. Palaeoclimatol.*, 305, 138–149, <https://doi.org/10.1016/j.palaeo.2011.02.027>, 2011.
- Śliwińska, K. K., Thomsen, E., Schouten, S., Schoon, P. L., and Heilmann-Clausen, C.: Climate-and gateway-driven cooling of Late Eocene to earliest Oligocene sea surface temperatures in the North Sea Basin, *Sci. Rep.*, 9, 4458, <https://doi.org/10.1038/s41598-019-41013-7>, 2019.
- Slotnick, B. S. and Schellenberg, S. A.: Biotic response of Tethyan bathyal ostracodes through the Eocene–Oligocene Transition: The composite faunal record from the Massicore and Massignano Global Stratotype Section and Point (east central Italy), *Mar. Micropaleontol.*, 103, 68–84, <https://doi.org/10.1016/j.marmicro.2013.03.005>, 2013.
- Sluijs, A. and Brinkhuis, H.: High Arctic late Paleocene and early Eocene dinoflagellate cysts, *J. Micropaleontol.*, 43, 441–474, <https://doi.org/10.5194/jm-43-441-2024>, 2024.
- Sluijs, A., Pross, J., and Brinkhuis, H.: From greenhouse to icehouse; organic-walled dinoflagellate cysts as paleoenvironmental indicators in the Paleogene, *Earth-Sci. Rev.*, 68, 281–315, <https://doi.org/10.1016/j.earscirev.2004.06.001>, 2005.
- Soták, J.: Paleoenvironmental changes across the Eocene–Oligocene boundary: insights from the Central-Carpathian Paleogene Basin, *Geol. Carpath.*, 61, 393–418, <https://doi.org/10.2478/v10096-010-0024-1>, 2010.
- Soutter, E. L., Kane, I. A., Martínez-Doñate, A., Boyce, A. J., Stacey, J., and Castelltort, S.: The Eocene–Oligocene climate transition in the Alpine foreland basin: Paleoenvironmental change recorded in submarine fans, *Palaeogeogr. Palaeoclimatol.*, 600, 111064, <https://doi.org/10.1016/j.palaeo.2022.111064>, 2022.
- Stärz, M., Jokat, W., Knorr, G., and Lohmann, G.: Threshold in North Atlantic–Arctic Ocean circulation controlled by the subsidence of the Greenland–Scotland Ridge, *Nat. Commun.*, 8, 15681, <https://doi.org/10.1038/ncomms15681>, 2017.
- Stockmarr, J.: Determination of spore concentration with an electronic particle counter, *Danmarks Geol. Undersø.*, 15, 87–89, <https://doi.org/10.22008/gpub/38152>, 1973.
- Stover, L. E. and Hardenbol, J.: Dinoflagellates and depositional sequences in the lower Oligocene (Rupelian) Boom clay formation, Belgium, *Bulletin de la Société belge de Géologie*, 102, 5–77, 1993.
- Straume, E. O., Steinberger, B., Becker, T. W., and Faccenna, C.: Impact of mantle convection and dynamic topography on the Cenozoic paleogeography of Central Eurasia and the West Siberian Seaway, *Earth. Planet. Sc. Lett.*, 630, 118615, <https://doi.org/10.1016/j.epsl.2024.118615>, 2024.
- Street, C. and Bown, P. R.: Palaeobiogeography of early Cretaceous (Berriasian–Barremian) calcareous nannoplankton, *Mar. Micropaleontol.*, 39, 265–291, [https://doi.org/10.1016/S0377-8398\(00\)00024-4](https://doi.org/10.1016/S0377-8398(00)00024-4), 2000.
- Švábenická, L.: *Braarudosphaera*-rich sediments in the Turonian of the Bohemian Cretaceous Basin, Czech Republic, *Cretaceous*

- Res., 20, 773–782, <https://doi.org/10.1006/cres.1999.0182>, 1999.
- Thierstein, H. R., Cortés, M. Y., and Haidar, A. T.: Plankton community behavior on ecological and evolutionary time-scales: when models confront evidence, in: *Coccolithophores: from molecular processes to global impact*, edited by: Thierstein, H. R. and Young, J. R., Springer, Berlin Heidelberg, 455–479, https://doi.org/10.1007/978-3-662-06278-4_17, 2004.
- Toffanin, F., Agnini, C., Rio, D., Acton, G., and Westerhold, T.: Middle Eocene to early Oligocene calcareous nannofossil biostratigraphy at IODP Site U1333 (equatorial Pacific), *Micropaleontology*, 59, 69–82, <http://www.jstor.org/stable/24413317>, 2013.
- Toledo, F. A., Cachão, M., Costa, K. B., and Pivel, M. A.: Planktonic foraminifera, calcareous nannoplankton and ascidian variations during the last 25 kyr in the Southwestern Atlantic: A paleoproductivity signature?, *Mar. Micropaleontol.*, 64, 67–79, <https://doi.org/10.1016/j.marmicro.2007.03.001>, 2007.
- Tulan, E., Sachsenhofer, R. F., Tari, G., Flecker, R., Fairbank, V., Pupp, M., and Ickert, R. B.: Source rock potential and depositional environment of the Lower Oligocene İhsaniye Formation in NW Turkey (Thrace, Karaburun), *Turk. J. Earth Sci.*, 29, 64–84, <https://doi.org/10.3906/yer-1906-14>, 2020.
- Turgut, S.: Evolution of the Thrace sedimentary basin and its hydrocarbon prospectivity, in: *Generation, accumulation, and production of Europe's hydrocarbons*, edited by: Spencer, M. A., Springer Berlin, Heidelberg, 415–437, ISBN 978-3-662-07417-6, 1991.
- Vahlenkamp, M., Niezgodzki, I., De Vleeschouwer, D., Lohmann, G., Bickert, T., and Pälike, H.: Ocean and climate response to North Atlantic seaway changes at the onset of long-term Eocene cooling, *Earth Planet. Sc. Lett.*, 498, 185–195, <https://doi.org/10.1016/j.epsl.2018.06.031>, 2018.
- van Der Boon, A., van der Ploeg, R., Cramwinckel, M. J., Kuiper, K. F., Popov, S. V., Tabachnikova, I. P., Palcu, D. V., and Krijgsman, W.: Integrated stratigraphy of the Eocene–Oligocene deposits of the northern Caucasus (Belaya River, Russia): Intermittent oxygen-depleted episodes in the Peri-Tethys and Paratethys, *Palaeogeogr. Palaeoclimatol.*, 536, 109395, <https://doi.org/10.1016/j.palaeo.2019.109395>, 2019.
- Van Mourik, C. A. and Brinkhuis, H.: The Massignano Eocene–Oligocene golden spike section revisited, *Stratigraphy*, 2, 13–30, <https://doi.org/10.29041/strat.02.1.01>, 2005.
- Van Simaëys, S., Brinkhuis, H., Pross, J., Williams, G. L., and Zachos, J. C.: Arctic dinoflagellate migrations mark the strongest Oligocene glaciations, *Geology*, 33, 709–712, <https://doi.org/10.1130/G21634.1>, 2005.
- Varol, O.: Didemnid ascidian spicules from the Arabian Peninsula, *J. Nannoplankton Res.*, 28, 35–55, <https://doi.org/10.58998/jnr2258>, 2006.
- Vermeesch, P.: IsoplotR: A free and open toolbox for geochronology, *Geosci. Front.*, 9, 1479–1493, <https://doi.org/10.1016/j.gsf.2018.04.001>, 2018.
- Vermeesch, P.: On the treatment of discordant detrital zircon U–Pb data, *Geochronology*, 3, 247–257, <https://doi.org/10.5194/gchron-3-247-2021>, 2021.
- Viganò, A., Coxall, H. K., Holmström, M., Vinco, M., Lear, C. H., and Agnini, C.: Calcareous nannofossils across the Eocene–Oligocene transition at Site 756 (Ninetyeast Ridge, Indian Ocean): implications for biostratigraphy and paleoceanographic clues, *Newsl. Stratigr.*, 56, 187–223, <https://doi.org/10.1127/nos/2022/0725>, 2023a.
- Viganò, A., Westerhold, T., Bown, P. R., Jones, T. D., and Agnini, C.: Calcareous nannofossils across the Eocene–Oligocene transition: Preservation signals and biostratigraphic remarks from ODP Site 1209 (NW Pacific, Shatsky Rise) and IODP Hole U1411B (NW Atlantic Ocean, Newfoundland Ridge), *Palaeogeogr. Palaeoclimatol.*, 629, 111778, <https://doi.org/10.1016/j.palaeo.2023.111778>, 2023b.
- Viganò, A., Dallanave, E., Alegret, L., Westerhold, T., Sutherland, R., Dickens, G. R., Newsam, C., and Agnini, C.: Calcareous nannofossil biostratigraphy and biochronology across the Eocene–Oligocene transition: the record at IODP Site U1509 (Tasman Sea) and a global overview, *Newsl. Stratigr.*, 57, 1–23, <https://doi.org/10.1127/nos/2023/0751>, 2024a.
- Viganò, A., Dallanave, E., Alegret, L., Westerhold, T., Sutherland, R., Dickens, G. R., Newsam, C., and Agnini, C.: Calcareous nannofossils and paleoclimatic evolution across the Eocene–Oligocene transition at IODP Site U1509, Tasman Sea, Southwest Pacific Ocean, *Paleoceanogr. Paleoclimatol.*, 39, e2023PA004738, <https://doi.org/10.1029/2023PA004738>, 2024b.
- Villa, G., Fioroni, C., Pea, L., Bohaty, S., and Persico, D.: Middle Eocene–late Oligocene climate variability: calcareous nannofossil response at Kerguelen Plateau, Site 748, *Mar. Micropaleontol.*, 69, 173–192, <https://doi.org/10.1016/j.marmicro.2008.07.006>, 2008.
- Villa, G., Fioroni, C., Persico, D., Roberts, A. P., and Florindo, F.: Middle Eocene to late Oligocene Antarctic glaciation/deglaciation and Southern Ocean productivity, *Paleoceanogr. Paleoclimatol.*, 29, 223–237, <https://doi.org/10.1002/2013PA002518>, 2014.
- Villa, G., Florindo, F., Persico, D., Lurcock, P., de Martini, A. P., Jovane, L., and Fioroni, C.: Integrated calcareous nannofossil and magnetostratigraphic record of ODP Site 709: Middle Eocene to late Oligocene paleoclimate and paleoceanography of the Equatorial Indian Ocean, *Mar. Micropaleontol.*, 169, 102051, <https://doi.org/10.1016/j.marmicro.2021.102051>, 2021.
- Waddell, L. M. and Moore, T. C.: Salinity of the Eocene Arctic Ocean from oxygen isotope analysis of fish bone carbonate, *Paleoceanography*, 23, 1–14, <https://doi.org/10.1029/2007PA001451>, 2008.
- Wade, B. S. and Bown, P. R.: Calcareous nannofossils in extreme environments: the Messinian salinity crisis, Poles Basin, Cyprus, *Palaeogeogr. Palaeoclimatol.*, 233, 271–286, <https://doi.org/10.1016/j.palaeo.2005.10.007>, 2006.
- Wade, B. S. and Pälike, H.: Oligocene climate dynamics, *Paleoceanography*, 19, 1–16 <https://doi.org/10.1029/2004PA001042>, 2004.
- Wei, W. and Wise Jr., S. W.: Biogeographic gradients of middle Eocene–Oligocene calcareous nannoplankton in the South Atlantic Ocean, *Palaeogeogr. Palaeoclimatol.*, 79, 29–61, [https://doi.org/10.1016/0031-0182\(90\)90104-F](https://doi.org/10.1016/0031-0182(90)90104-F), 1990.
- Wei, W., Villa, G., and Wise Jr., S. W.: Paleoceanographic implications of Eocene–Oligocene calcareous nannofossils from sites 711 and 748 in the Indian Ocean, *Proc. Ocean Drill. Progr. Sci. Res.*, 120, 979–999, <https://doi.org/10.2973/odp.proc.sr.120.199.1992>, 1992.

- Williams, G. L., Fensome, R. A., and MacRae, R. A.: The Lentin and Williams Index of Fossil Dinoflagellate 2019 Edition, AASP Contributions Series Number, 50, 1173, ISSN 0160-8843, 2019.
- Winter, A. and Siesser, W. G. (Eds.): *Coccolithophores*, Cambridge Univ. Press, Cambridge, 242 pp., ISBN 0-521-38050-2, 1994.
- Yücel, A. O., Özcan, E., and Erbil, Ü.: Latest Priabonian larger benthic foraminiferal assemblages at the demise of the Soğucak Carbonate Platform (Thrace Basin and Black Sea shelf, NW Turkey): implications for the shallow marine biostratigraphy, *Turk. J. Earth Sci.*, 29, 85–114, <https://doi.org/10.3906/yer-1904-19>, 2020.
- Zachos, J. C., Quinn, T. M., and Salamy, K. A.: High-resolution (104 years) deep-sea foraminiferal stable isotope records of the Eocene–Oligocene climate transition, *Paleoceanography*, 11, 251–266, <https://doi.org/10.1029/96PA00571>, 1996.
- Zachos, J., Pagani, M., Sloan, L., Thomas, E., and Billups, K.: Trends, rhythms, and aberrations in global climate 65 Ma to present, *Science*, 292, 686–693, <https://doi.org/10.1126/science.1059412>, 2001.
- Ziveri, P., Baumann, K. H., Böckel, B., Bollmann, J., and Young, J. R.: Biogeography of selected Holocene coccoliths in the Atlantic Ocean, in: *Coccolithophores: from molecular processes to global impact*, edited by: Thierstein, H. R. and Young, J. R., Springer, Berlin Heidelberg, 403–428, https://doi.org/10.1007/978-3-662-06278-4_15, 2004.
- Zonneveld, K. A., Marret, F., Versteegh, G. J., Bogus, K., Bonnet, S., Bouimetarhan, I., Crouch, E., de Vernal, A., Elshanawany, R., Edwards, L., Esper, O., Forke, S., Grøsfjeld, K., Henry, M., Holzwarth, U., Kielt, J.-F., Kim, S.-Y., Ladouceur, S., Ledu, D., Chen, L., Limoges, A., Londeix, L., Hu, S.-H., Mahmoud, M. S., Marino, G., Matsouka, K., Matthiessen, J., Mildenhall, D. C., Mudie, P., Neil, H. L., Pospelova, V., Qi, Y., Radi, T., Richerol, T., Rochon, A., Sangiorgi, F., Solignac, S., Turon, J.-L., Verleye, T., Wang, Y., Wang, Z., and Young, M.: Atlas of modern dinoflagellate cyst distribution based on 2405 data points, *Rev. Palaeobot. Palyno.*, 191, 1–197, <https://doi.org/10.1016/j.revpalbo.2012.08.003>, 2013.